AD NUMBER
ADB282747
NEW LIMITATION CHANGE
TO Approved for public release, distribution unlimited
FROM Distribution authorized to U.S. Gov't. agencies only; Proprietary Information; Dec 2001. Other requests shall be referred to US Army Medical Research and Materiel Command, 504 Scott Street, Fort Detrick, MD 21702
AUTHORITY
USAMRMC ltr, 11 Mar 2003

AD_____

Award Number: DAMD17-00-1-0054

TITLE: Development of a Computer-Aided Diagnostic System for the
Detection of Lung Cancer in Helical CT

PRINCIPAL INVESTIGATOR: Shih-Chung Ben Lo, Ph.D.

CONTRACTING ORGANIZATION: Georgetown University Medical Center
                           Washington, DC 20007

REPORT DATE: December 2001

TYPE OF REPORT: Final

PREPARED FOR: U.S. Army Medical Research and Materiel Command
               Fort Detrick, Maryland 21702-5012

The views, opinions and/or findings contained in this report are
those of the author(s) and should not be construed as an official
Department of the Army position, policy or decision unless so
designated by other documentation.

NOTICE

THIS TECHNICAL REPORT HAS BEEN REVIEWED AND IS APPROVED FOR PUBLICATION.

REPORT DOCUMENTATION PAGE	*Form Approved* *OMB No. 074-0188*

Public reporting burden for this collection of information is estimated to average 1 hour per response, including the time for reviewing instructions, searching existing data sources, gathering and maintaining the data needed, and completing and reviewing this collection of information. Send comments regarding this burden estimate or any other aspect of this collection of information, including suggestions for reducing this burden to Washington Headquarters Services, Directorate for Information Operations and Reports, 1215 Jefferson Davis Highway, Suite 1204, Arlington, VA 22202-4302, and to the Office of Management and Budget, Paperwork Reduction Project (0704-0188), Washington, DC 20503

1. AGENCY USE ONLY (Leave blank)	2. REPORT DATE December 2001	3. REPORT TYPE AND DATES COVERED Final (8 Nov 99 – 7 Nov 01)	

4. TITLE AND SUBTITLE Development of a Computer-Aided Diagnostic System for the Detection of Lung Cancer in Helical CT	5. FUNDING NUMBERS DAMD17-00-1-0054

6. AUTHOR(S)
Shih-Chung Ben Lo, Ph.D.

7. PERFORMING ORGANIZATION NAME(S) AND ADDRESS(ES) Georgetown University Medical Center Washington, DC 20007 E-mail: lo@isis.imac.georgetown.edu	8. PERFORMING ORGANIZATION REPORT NUMBER

9. SPONSORING / MONITORING AGENCY NAME(S) AND ADDRESS(ES) U.S. Army Medical Research and Materiel Command Fort Detrick, Maryland 21702-5012	10. SPONSORING / MONITORING AGENCY REPORT NUMBER

11. SUPPLEMENTARY NOTES

20020930 056

12a. DISTRIBUTION / AVAILABILITY STATEMENT Distribution authorized to U.S. Government agencies only (proprietary information, Dec 01). Other requests for this document shall be referred to U.S. Army Medical Research and Materiel Command, 504 Scott Street, Fort Detrick, Maryland 21702-5012.	12b. DISTRIBUTION CODE

13. ABSTRACT *(Maximum 200 Words)*

For a long time, lung cancer has been the leading cause of cancer death. Clinical evidences suggest that early detection of lung cancer can increase the chance of survival for those patients suffering lung cancer. Even patients with initial pulmonary metastasis, early detection will allow earlier modification of these patients' therapies incorporating early treatment of the metastases. Therefore, any method, that can improve the clinical efficacy in detecting lung cancer, is of serious public health interest.

Our research interest has been aimed specifically to assist radiologists in the diagnosis of lung cancer. We have developed methods in nodule modeling and analysis, segmentation of lung field and nodule suspects as well as image functions for segmentation of lung and enhanced 3-dimensional visualization of local nodule regions. We have also integrated majority our work and become a workstation for diagnostic of lung cancer in CT. The 3D topological characteristics of local structures including bronchi, blood vessels, and nodules can be computed and evaluated. When a location of a region of interest is identified, the computer can automatically compute size, and 3D display the suspected lesion. The system can also allow the user to perform interactive operation for evaluation of lung lesions.

14. SUBJECT TERMS Cancer Detection, Computer-Aided Diagnosis, Nodule Modeling, and Cancer analysis			15. NUMBER OF PAGES 51
			16. PRICE CODE

17. SECURITY CLASSIFICATION OF REPORT Unclassified	18. SECURITY CLASSIFICATION OF THIS PAGE Unclassified	19. SECURITY CLASSIFICATION OF ABSTRACT Unclassified	20. LIMITATION OF ABSTRACT Unlimited

NSN 7540-01-280-5500

Standard Form 298 (Rev. 2-89)
Prescribed by ANSI Std. Z39-18
298-102

(3)   Table of Contents

List of Personnel Receiving Pay from the Research Effort

1. Shih-Chung B. Lo, Ph.D.
2. Matthew T. Freedman, MD
3. Andrezj Delegacz, MS
4. Hui Zhao, MS
5. MedCrane LLC as a Subcontractor: Key Personnel is Dr. Huchen Xei

(4)   Introduction

4.1. Project Background

This is a project funded by Specified Appropriations Program Award (Award Category: Advanced Cancer Detection) and sponsored by United States Army Medical Research and Material Command (USMRMC). We originally proposed a two-year project. However, only the first year of the research program was granted. Official funding period was from November 8, 1999 to November 7, 2000. In spring of 2000, the PI encountered severe physical problem and had a major surgery resulting in some delay of project progress. In fall of 2000, a one-year no-cost extension was granted by the USMRMC for the research team to complete this project.

4.2. Clinical Background and Significance of the Research

Since the early 1990s, the volumetric CT technique has introduced virtually contiguous spiral scans that cover the chest in a few seconds. This technique has greatly reduced CT image artifacts caused by unequal respiratory cycles, partial volume, and cardiac motion. Newer models of the helical CT systems are capable of performing the scan and image reconstruction simultaneously. Detectability of pulmonary nodules has been greatly improved with this modality. High-resolution CT has also proved to be effective in characterizing edges of pulmonary nodules [Zwirewich 1991]. Zwirewich and his colleagues reported that shadows of nodule spiculation correlates pathologically with irregular fibrosis, localized lymphatic spread of tumor, or an infiltrative tumor growth; pleural tags represent fibrotic bands that usually are associated with juxtacicatrical pleural retraction; and low attenuation bubble-like patterns that are correlated with bronchioloalveolar carcinomas. These are common CT image patterns associated with malignant processes of lung masses. Because a majority of solitary pulmonary nodules (SPN) are benign, three main criteria are used for determination of benignancy: (a) high attenuation values distributed diffusely throughout the nodule, (b) a representative CT number of at least 164 HU, and (c) hamartomas are lesions 2.5 cm or less in diameter with sharp and smooth edges and a central focus of fat with CT number numbers of -40 to -120 HU. These reports suggest that there are features that a computer could use to differentiate benign and malignant lesions.

Our project in computer-aided diagnosis (CADx) is aimed specifically at the smallest of lung nodules, 3 to 20 mm, well within the size limits for T1 cancer (< 30 mm). If there is to be a detectable benefit in the use of the helical CT, it is likely to be in cancers at the lower limits of size detectable by radiologists, at or just below the radiographically detectable size.

Since lung cancer continues to exact a significant toll on the American population, and other methods of early detection have had only limited success, our continued efforts to improve the accuracy of interpretation of helical CT images and chest radiographs to be quite important. The helical CT represents an advanced clinical tool for high-risk patients. The chest radiograph continues to be the clinical tool for lung cancer detection whether in symptomatic or asymptomatic patients. When chest radiographs were read by two radiologists, the improved detection rate is well documented [Stitik 1985]. This clinical outcome suggests that our approach of using the computer as a second reader is clinically meaningful.

(5) Body of the Report

Because the change to a smaller scope program requested by the sponsor (USMRMC), we focused our tasks on the development of functional tools for diagnostic chest CT images in this project.

(A) Collection of Thoracic of CT Images

When using the diagnostic protocol, thin-slice CT images near the nodule area were acquired. At Georgetown, we are currently using a Siemens multislice multidetector helical CT system for thoracic CT examinations. The CT parameters were set at a 2 mm beam width, 2 mm/sec table speed, reconstruction interval of 1-2 mm between adjacent slices, and tube current of 150-200 mA. Each cross-sectional CT image is formatted at 512×512×12 bits. Typically, each helical CT produces 30 to 50 images per examination while scanning the selected area. The number of images can be as many as 300-500 images while scanning the entire chest. During the funding period, we have collected 74 cases. Of which 31 are lung cancer cases and 43 normal cases. In the normal cases, 38 of them have benign nodules. We have used these cases to develop diagnostic function tools and analytic algorithms.

In the same time, we also helped our industrial partner – Deus Technology LLC – to acquire a significant number of CT images from leading medical center in the country using their internal fund. So far, they have collected 621 cases: 73 lung cancer cases and 414 benign nodules were clinically identified. Our research team can access to this dataset for our long-team collaboration with the company.

Deus, a subsdiary of Caelum Research Corp., is a unique lung cancer CAD company and has been working in the field for ten years. Through many technical endeavors and collaboration with researchers at Georgetown University and University of Chicago, a commercial product resulting from this lung cancer CAD project has recently been approved by the FDA. The URL of the FDA website is at http://www.fda.gov/cdrh/pdf/p000041.html. The Georgetown team joined with the company design the clinical trial. The Georgetown team was also responsible for performing the MRMC ROC study and clinical tests using the CAD system. The CAD team at the University of Chicago was responsible for the ROC analysis. Both teams served as subcontractors to Deus during the clinical evaluation period as a part of activities seeking FDA approval.

(B) Segmentation of Lung Field in CT Images
B.1. Theory

Our research finding was initiated by training and analyzing the convolution neural network (CNN) [Lo 1995]. Although the CNN training usually takes a great deal of computation, it provides an effective solution between the input and target images. The solution is formatted as the internal kernels which function as convolution filters. Technically, these kernels can be composed into a single kernel. One can also deconvolve the original input image by the output image to obtain the filter that is equivalent to the CNN process. Although the resulting filters obtained from deconvolution process may not be identical from every pairs of input and output images, our experiment indicates that they are quite close as far as global segmentation of a large area is concerned for a specific type of images. To be exact, we found that a single linear filter can be found for each type of image segmentation mentioned above. In addition, all linear filters discovered so far belong to a single set of filter family.

Theoretical speaking, the frequency band associated with large area without detail structures should be predominated by low frequency. The results, obtained by composing the CNN kernel discussed above, prove this fact. We, therefore, hypothesize that the criteria of low frequency filters for global segmentation should contain (i) significant amounts of low frequency components, (ii) very few or no high frequency components, (iii) no band frequencies associated with the structures that are intended to be removed, and (iv) a low (or zero) mean coefficients (i.e., $\sum_{x,y} t(x,y) \approx 0$.) Although, a great deal of low frequency filter banks are available, there are three types of known filters commonly used in digital signal processing: (a) uniform low-pass filters in frequency domain, (b) local mean value operators (i.e., uniform column filter) in spatial domain, and (c) Gaussian shape filters. Since main frequency components in (a) can be approximately described by (b) and (c), we can assume that the filter to be constructed is composed of (b) and (c) components in this study.

$$t(x,y) = m(x,y) + G(x,y) \qquad \qquad \ldots(1)$$

where

$$m(x,y) = \begin{cases} w_1 & for \ (x^2+y^2)^{1/2} \leq r \\ 0 & for \ (x^2+y^2)^{1/2} > r \end{cases}, \quad G(x,y) = w_2 \exp\left(-(x^2+y^2)/2\sigma^2\right)$$

and r is the cut-off range of the uniform column filter. In addition, the uniform column filter possesses a property of $\pi r^2 w_1 = 1$. Substitute the components of the m(x,y) and G(x,y) filter in eq. (1), we have

$$t(x,y) = \begin{cases} w_1 + w_2 \exp\left(-(x^2+y^2)/2\sigma^2\right) & for \ (x^2+y^2)^{1/2} \leq r \\ w_2 \exp\left(-(x^2+y^2)/2\sigma^2\right) & for \ (x^2+y^2)^{1/2} > r \end{cases} \qquad \ldots(2)$$

We further constraint that the filter should be a zero mean filter (i.e., $\sum_{x,y} t(x,y) = 0$), which is a common requirement when designing an edge enhancement filter. With this constraint, a logical solution in eq. (1) is

$$\pi r^2 w_1 = -w_2 \iint_{x,y} \exp\left(-(x^2+y^2)/2\sigma^2\right) = 1. \qquad \qquad \ldots(3)$$

Hence, $w_1 = \dfrac{1}{\pi r^2}$ and $w_2 = \dfrac{-1}{2\pi\sigma^2}$. Substitute them into eq. (2), we have

$$t(x,y) = \begin{cases} \dfrac{1}{\pi r^2} - \dfrac{1}{2\pi\sigma^2} \exp\left(-(x^2+y^2)/2\sigma^2\right) & for \ (x^2+y^2)^{1/2} \leq r \\ \dfrac{-1}{2\pi\sigma^2} \exp\left(-(x^2+y^2)/2\sigma^2\right) & for \ (x^2+y^2)^{1/2} > r \end{cases} \qquad \ldots(4)$$

Our initial experience indicates that the size of the largest structure to be removed should be greater than 2r but smaller than 2σ.

B.2. Determination of the filter parameters

We initially set parameters $2r = 2$ cm and $2\sigma = 5$ cm which led to $w_1 = 0.3183109886 \text{cm}^{-2}$ and $w_2 = -0.02546479 \text{ cm}^{-2}$. After some heuristic tuning based on observation of 50 CT filtered images, we determines that $2r = 1.26$ cm and $2\sigma = 5.18$ cm which induce $w_1 = 0.7771237 \text{ cm}^{-2}$ which is equivalent to $0.003807906 \text{ (pixel)}^{-1}$ and $w_2 = -0.023725785 \text{ cm}^{-2}$ which is equivalent to $0.000116256 \text{ (pixel)}^{-1}$. However, in our digital implementation, $w_1 = 0.004016 \text{ (pixel)}^{-1}$ and $w_2 = -0.000116256 \text{ (pixel)}^{-1}$. The difference in w_1 is because that small circle area possesses a large imperfection of the partial area pixel effect.

With digital implementation, we replace FT by discrete Fourier transform (DFT) and replace IFT with inverse discrete Fourier transform (IDFT). The digital form of the filter becomes

$$
t(x,y) = \begin{cases} \dfrac{1}{A_m} - \dfrac{1}{A_G}\exp\!\left(-(x^2+y^2)/2\sigma^2\right) & \text{for} \quad (x^2+y^2)^{1/2} \le r \\[2ex] \dfrac{-1}{A_G}\exp\!\left(-(x^2+y^2)/2\sigma^2\right) & \text{for} \quad (x^2+y^2)^{1/2} > r \end{cases} \quad \ldots(5)
$$

where $A_m = \sum_{x,y} 1 \quad \text{for} \quad (x^2+y^2)^{1/2} \le r$ and $A_G = \sum_{x,y} \exp\!\left((x^2+y^2)/2\sigma^2\right)$

Since the size of each pixel is 0.7 mm, $2r$ is equivalent to 18 pixels (1.26 cm) in the flat column filter and 2σ is 74 pixels (5.18 cm) in the Gaussian filter. Hence, $A_m = 249$ and $A_G = 8,602$. These parameters were determined with consideration of trimming large vessels. This composed 2-D filter is named invert umbrella filter. Figure 1 shows the filter design intrigued by the convolution neural network processing. Figure 2 shows an example of the CT images with a large abnormality pattern and its filtered image.
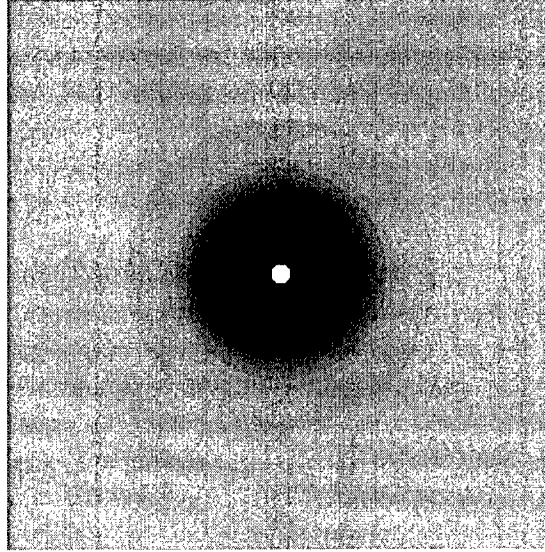

Figure 1. Filter designed for the segmentation of lung in chest radiography (B). Note that the filtered image is scaled to 255 for highest values for the display purposes which means the scaling factor is $(255A_m)$.

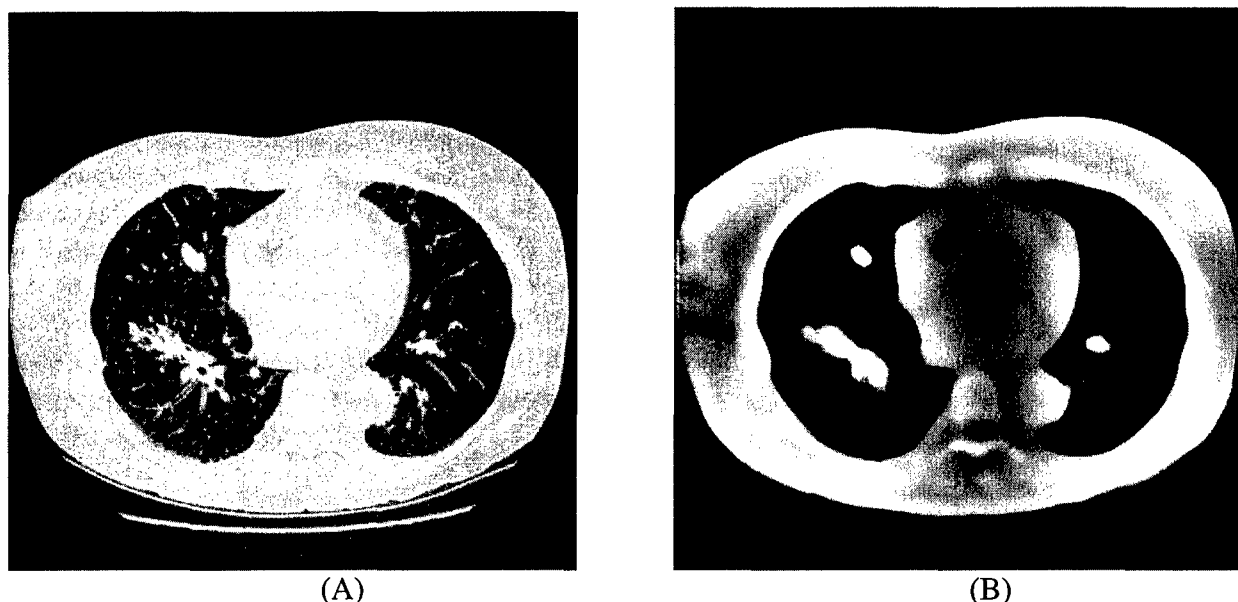(A)   (B)

Figure 2. The original CT chest image (A) and its segmented image (B) filtered by Figure 1(B).

B.3. Segmentation of Lung and Its Applications

The next step of segmentation was to find the contours of the lung field from the slices processed with the segmentation filter. We used the contour tracking method for this purpose. We observed that sometimes the contours of the lung field obtained with use of the filter covered an area slightly larger than actual lung field. To account for this artifact, we chose to apply the contouring algorithm more than once (usually 3-5 times) in a sequential order where the input slice to the contouring procedure in the current run was the output from the previous run (except the first run). In the last step of the segmentation, we used the last version of the contour as a template to extract the lung field on the original CT image. Figure 3 shows the whole segmentation path for a single slice.

Since lung parenchyma is the primary area of interest in the detection of lung cancer, segmentation of lung region has a lot of application particularly in the field of automatic computer functions and analyses, for example, (i) automatic lung cancer detection, (ii) automatic image enhancement of lung and mediastinum regions, (iii) 3-D image viewing of lung etc. We will report the result of 3-D image of lung in section (C). Section B.4 reports the application in automatic image enhancement of lung and mediastinum regions.

B.4. Development of dual-window display functions for clinical viewing

In the current clinical practice, CT images shown on the monitor are read twice with two window-level settings: lung and mediastinum windows. We have developed a dual-window function that can automatically produces artifact-free CT images (processed from the original CT) for clinical reading in a screening program. With this computer-assisted function, we can expect that the radiologist's reading time in lung CT screening will be dramatically reduced. A similar function can be applied to other medical imaging such as chest radiography.

For all thoracic CT cases come into the workstation, the images can be processed by a computer program that is capable of automatically segmenting lung and non-lung areas. In the screening mode, an automatic processing using the dual window/level function is recommended. The coordinates of the segmented boundary were stored as a file. When dual window/level

function was called, each CT slice and its corresponding lung boundary were loaded to the computer program. Window/level settings for lung and mediastinum was then applied at the corresponding areas respectively to generate an enhanced image for a single clinical reading. Figure 3 shows an example of this potential clinical display function. The lung boundary also can be used for other display and computer-aided functions.

The technical development was mainly on automatic segmentation of the lungs. Since this procedure serve as fundamental information for display and computer-aided functions, attention was paid to a number of important points: (1) the appearance of solid pulmonary nodules (SPNs) along the chest wall, (2) inaccuracy of delineation on the boundary between the chest wall and lung, and (3) inaccuracy of delineation on the boundary between the lung and liver, (4) hilum and bronchus near the heart may contain lung nodules, which may require a more sophisticated segmentation procedure. The filter based boundary detection method possesses a trimming mechanism that can automatic cut the branches of a smooth curve. Nodules and bronchi less than 3 cm were removed in the lung regions in the filtered images to facilitate the computer delineation. The boundary detection for the lung region includes nodules and bronchi as demonstrated in Figures 3(A) - 3(C).

| (A) Original | (B) IUF filtered image | (C) Delineation of the lungs |

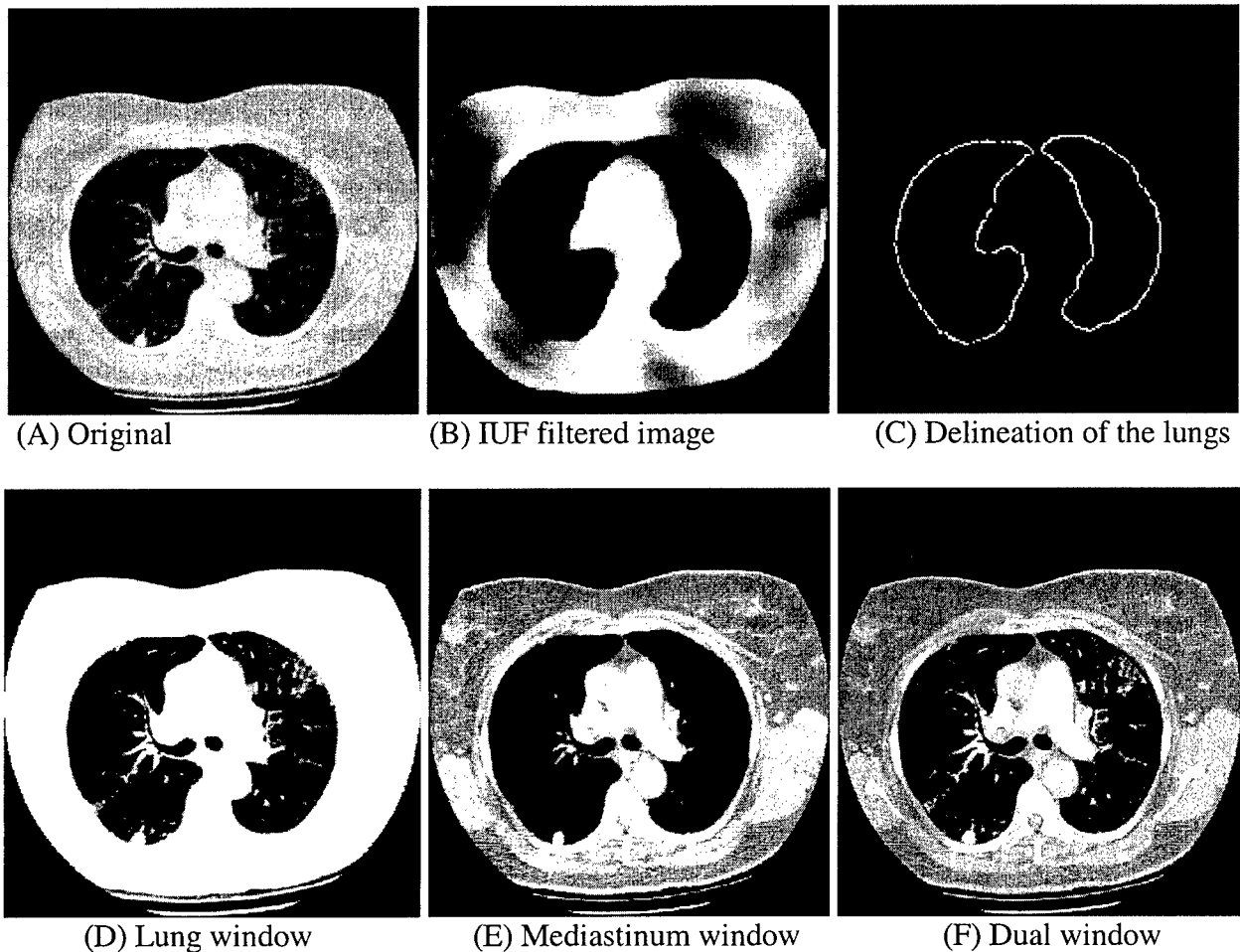| (D) Lung window | (E) Mediastinum window | (F) Dual window |

Figure 3. Dual-window single display optimized for lung and mediastinum in the same CT slice. It allows the reading of both lung-enhanced (D), mediastinum-enhanced (E), and CT in a single display (F). This is based on the IUF technique that can capture global region of interest and lead to robust delineation of the lungs.

(C) Modeling and Analysis of Lung Nodules
C.1. Superquadrics Deformable Model

We have used a superquadrics deformable technique, which is a parameterized model [Ballard 1981; Barr 1981; Terzopoulos 1991], to study the nodules and vessels. The superquadrics deformable method can describe the surface of a 3D object with a set of thirteen parameters. By modifying the parameters, the shape of the 3D object is deformed accordingly. The geometric characteristics of an object can be represented by the thirteen parameters. In using this model, the goal is to establish a reference configuration for the extracted contour data points. The thirteen parameters describe the geometric characteristics of an object with its location, orientation, size, squareness, and tapering. Specifically, these parameters are: (1) x, (2) y, and (3) z coordinates of the central point of an object; the angles at which the object is situated in the (4) x-, (5) y-, and (6) z-axes describe the orientation; the radius of the (7-9) three directions depicts the size; the squareness (10) one in the xy-plane (ε_1) and (11) one in the xz-plane (ε_2); and the last two parameters are about tapering in the (12) x- and (13) y-axes. In this study, the shapes of the target objects are either spherical or tubular, thus the parameters of squareness and tapering will be fixed and the rest of nine parameters will remain flexible to represent the surface function of the object, F.

C.2. Spatial Correlation and Differential Ratio

For a given target object within the pulmonary region, a seed object grows within the target object. In this study, the seed starts as a small tube object. We define a cost function, Eq. (1), as a correlation measurement between the seed object and the target. If the seed object derived from a parameter set perfectly fits N contour points (xi, yi, zi) in the target object, where i=1,2,3..., N, the output value of the cost function is zero. In other words, when the output value is smaller, the similarity between the deformed object and the target object is higher. Conversely, when the output value is larger, the two objects are less similar. In this study, a cost value (C_b) was calculated before the seed object is deformed. During the iteration of the deformation process, a Powell's quadratically convergent method was introduced to obtain the optimal parameter set [Press 1992]. Once the optimal object is available, another cost value (C_a) is then calculated. The cost function is given below:

$$C = \sum_{i=1}^{N} \left[1 - F(x_i, y_i, z_i; a_1, \dots, a_9) \right]^2 \qquad \dots(6)$$

Our method for determining the shape of a given target object is based on a cost ratio:
$$R = C_a / C_b \qquad \dots(7)$$

The seed is a tubular shaped object and the parameters of squareness and tapering are fixed during the deformation process. For this reason, the optimized seed object can fit a tubular target object better than a spherical object. In other words, C_a will be much smaller than C_b for tubular target objects. As a result, the cost ratio, R, would be a small number. For a spherical target object, the difference between C_a and C_b will be relatively small. A result would thus be a large R value.

Based on this algorithm development tailored for extracting lung structures, we have processed a set of CT image slab containing 16 contiguous chest slices. The 3D visualization of blood vessels, airways, and nodules by volume rendering of these test objects are shown in Figures 4 and 5. The R values of the objects are listed in Table 1. It is obvious that object 18 has a low cost ratio, 0.967; thus, it is determined to be a round object (e.g., nodule).

Table 1: R values of the 18 objects

Objects	1	2	3	4	5	6	7	8	9
R values	0.168	0.243	0.301	0.175	0.369	0.519	0.307	0.214	0.445
Identification	Vessel Or Airway	Vessel Or Airway	Vessel Or Airway	Vessel Or Airway	Vessel Or Airway	Vessel Or Airway	Vessel Or Airway	Vessel Or Airway	Vessel Or Airway

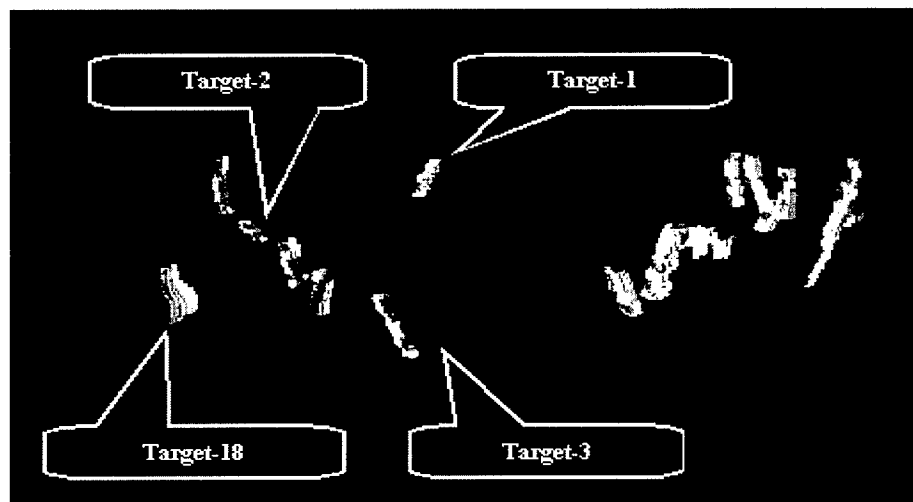| Objects	10	11	12	13	14	15	16	17	18
R values	0.456	0.668	0.327	0.455	0.582	0.203	0.345	0.275	0.967
Identification	Vessel Or Airway	Vessel Or Airway	Vessel Or Airway	Vessel Or Airway	Vessel Or Airway	Vessel Or Airway	Vessel Or Airway	Vessel Or Airway	Lung Nodule

Figure 4. Segmented target objects using the superquadrics deformable model in a slab of pulmonary region.

Figure 5. 3-D visualization of isolated target objects in a pulmonary region: (a) target object 1, (b) target object 2, (c) target object 3, and (d) target object 18.

D. Volumetric display of CT images for lung cancer diagnosis

We have developed a sequence of function tools to remove the appearances of the chest wall, heart, mediastinum, and diaphragm from the CT images. The lung parenchyma rendered as 3D slices can be reconstructed to form a 3-D slab presentation. Since the lung density is low, 3D transparent views from different angles are possible. This isotropic 3D transparent representation can be used to facilitate radiologists' searching for nodules in "thin-section" thoracic screening CT. A mouse and defined keys were made available for the radiologist to control display features, such as the angle, CT number threshold, slice viewing, virtual operation (image clipping), and distance measurement. The computer also highlight the nodules detected by the computer in the CT volumetric display.

We are in the process to evaluate the clinical efficacy of this viewing method in two steps by: (1) provide the volume rendering only as a display tool for an initial clinical viewing, and (2)

highlight the detected nodule in the volume of the 3D display. At this moment, it is premature to assess the clinical role of this display method.

For the analysis of a focal suspected abnormality, our radiologists consider that the slab appears to contain more information than appears to be necessary. The eventual goal will be to have a cube measuring 50-100 pixels on each side of the cube and centered on the identified abnormality displayed in 3D to assist the radiologists in diagnosis. Decreasing the volume of the slab to a cube will decrease the number of overlapping shadows and thereby should increase the speed of the radiologists in their evaluation.

With 3-D display capability developed in this laboratory, we have also implemented a virtual broncoscopy capability. This display module will be of great value for investigation of the central lung cancer. Figure 6 shows a part of segmented bronchial tree using a set of thoracic CT images (7mm per slice). The arrow on the upper middle section of the 3D volume rendering images shows the position of the virtual bronchoscopy. The bronchial airway view of virtual bronchoscopy is shown on the right-upper corner in Figure 6. The transverse CT image was selected from the original set corresponding to the position of arrow base. The lower-bottom image was the interpreted sagital CT image corresponding to the upper rectangle box area on the 3D volume rendering image. With a set of high-resolution thoracic CT images (e.g., 1-2 mm per slice), finer structures of the lumen, smaller bronchi, and vessels can be presented using this prototype function.
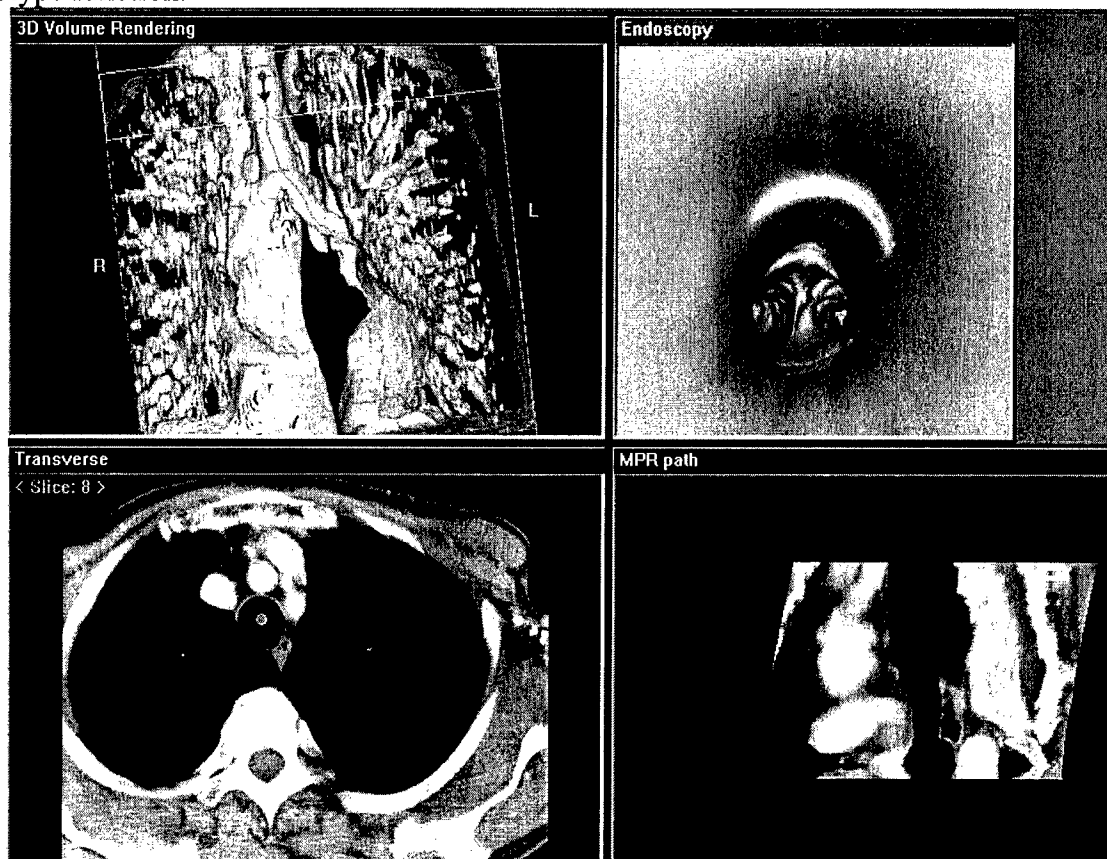

Figure 6. Segmentation of bronchial tree (upper-left) and it potential use as a virtual bronchoscopy (upper-right). The transverse section (lower-left) and sagital view of a section (lower-right) are shown in corresponding to the arrow and the rectangle box level of the CT images, respectively. Movie display can be made for tracing the bronchial airway through sequence of virtual bronchoscopy display.

E. Local 3-D Visualization and Processing of Nodules

Clinically, a thin-section thoracic CT of the patient is used when the radiologist observes a significant indication of potential lung cancer in the thick-slice (typically low-dose) CT images or in chest radiographs. We have developed an interactive 3D image processing method to enhance the features embedded in the thin-slice CT images. The tissue pattern and vascularture of blood vessels near the lung nodule play important roles for the radiologist to correlate the radiological and macro-pathological signs. For a single nodule appearing in a number of consecutive CT slices, an automatic segmentation algorithm was developed to characterize the nodule's volume in 3D. First, the location of a nodule of interest is manually selected by the radiologist, or automatically input from the detection part of the system. Once an object of interest is identified, a seed location is determined as the center of gravity based on the volume of interest (VOI).

From this local image window, the computer would determine the threshold for binarizing the gray level image. Once the image is binarized, the morphological process is used to smooth and prune the unnecessary connections. An efficient connected component analysis method is developed to analyze the possible connections of neighbor voxels. Adjacency matrices and complement graphs are constructed to identify those patterns of neighbor voxel connections that are possible, while redundant combinations are thus eliminated. It utilizes the adjacency relation of visited neighbors to construct a connectivity chart. Using this chart to examine each connected component within the 3D image, all the connected voxels in the same region can be labeled accordingly.

This connected component labeling is used to isolate the smaller structure from the largest object within the binarized image. After the smaller structure is extracted and initial contours are traced, an intensity profile was then measured under each extracted contour. The continuity of the intensity profile is calculated to adjust the smoothness of the final contour. The volume size, longest and shortest axes, average intensity, centroid location, etc., of the final object was then computed. If there is one nodule identified and measured in two different scans, the expected nodule doubling time will also be computed. Figure 7 shows an isolated lung nodule and the nodule without vessels processed by the pruning for measurement of nodule size. We are still working on the seprartion of small nodule from attached bronchus or vessel that requires high degree of segmentation accuracy. An example of unseparatbale nodule and bronchus is shown in Figure 8.
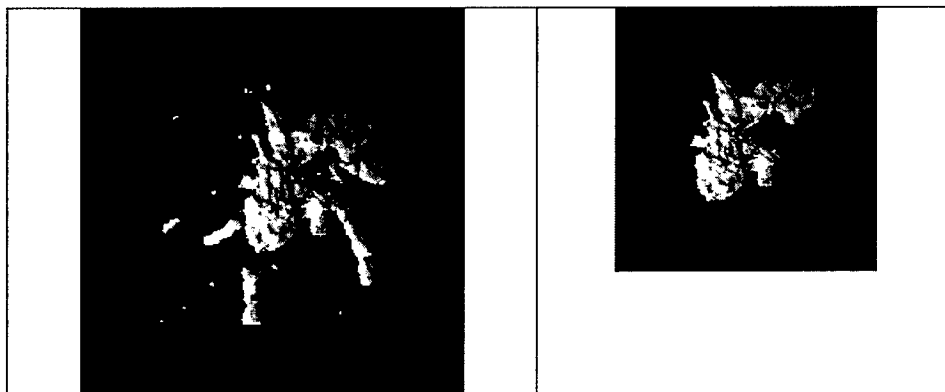

Figure 7. An isolated lung nodule, which is a malignant tumor, and its vicinity vessels in (a) and after the pruning the vicinity vessels in (b). **Real-time display version containing vessels is used for radiologist's diagnostic viewing. For the computation of nodule size, we however would use the pruning version of the nodule.**
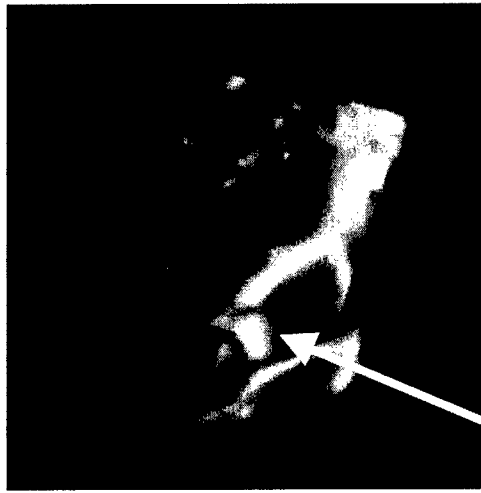
13

Figure 8. A small benign nodule that is almost unseparatbale from a bronchus.

F. Integration of Function Tools as a Dedicated Lung Cancer Diagnostic Module

Besides the nodule analysis research and development of function tools described above, we have also implemented majority of our work in a workstation prototype that is current under clinical evaluation. The system composed 2D display, basic image processing tools, segmentation of lung field, segmentation of lung nodules, surface rendering, 3D volume rendering, overlay of objects for 2D or 3D display. In addition, the local 3D visualization function with zooming and panning capability is also included in the system. The Appendix of this report containing 15 figures shows a part of the system function capability.

(6) Key Research Accomplishments

- Developed a robust segmentation method using invert umbrella filter for delineation of lung field in CT images.

- Developed a superqudratic modeling technique to analysis of lung nodules.

- Developed functional tools for 2D and 3D CT image display.

- Developed method for Local 3-D Visualization and Processing of Nodules.

- Integrated the developed function tools and a part of research outcomes in a Lung Cancer Detection Workstation.

- Developed the graphical user interface for the Lung Cancer Detection Workstation.

- Published two papers related to this project.

14

(7) Reportable Outcomes

<u>Publications</u>

Delegacz A., Lo S.C., Choi J.J., Xei H.C., Freedman M.T., and Mun S.K. "Three-Dimensional Visualization System as an Aid for Lung Cancer Diagnosis," SPIE Proc. Med. Imag., Vol. 3976, 2000, pp. 401-409.

Delegacz A., Lo S-C. B., Freedman M.T., and Mun S.K. "Feature Extraction, Analysis, and 3D Visualization of Local Region in Volumetric CT Images," SPIE Med. Imag., Vol. 4319, 2001, pp. 76-81.

<u>Oral Presentation</u>

Delegacz A., Lo S.C., Choi J.J., Xei H.C., Freedman M.T., and Mun S.K., "Three-Dimensional Visualization System as an Aid for Lung Cancer Diagnosis," Presented in 2000 SPIE Medical Imaging in San Diego, California.

Delegacz A., Lo S-C. B., Freedman M.T., and Mun S.K., "Feature Extraction, Analysis, and 3D Visualization of Local Region in Volumetric CT Images," Presented in 2001 SPIE Medical Imaging in San Diego, California.

Lo S.C., Freedman M.T., Delegacz A.M., Lure Y.M., and Xei H.C., "Computer-Aided Viewing for Lung Cancer Diagnosis in Helical Thoracic CT," Presented in IRT (Integrated Research and Technology – September 21-23, 2000) Sponsored by TATRC in Fort Detrick, Maryland.

(8) Conclusions

We have developed methods in nodule modeling and analysis, segmentation of lung field and nodule suspects as well as image functions for segmentation of lung and enhanced 3-dimensional visualization of local nodule regions. We have also integrated majority our work and become a workstation for diagnostic of lung cancer in CT. The system is aimed to assist the radiologist in the analysis of lung nodules.

The 3D topological characteristics of local structures including bronchi, blood vessels, and nodules can be computed and evaluated. When a location of a region of interest is identified, the computer can automatically compute size, surface of the area, and normalized shape index of the suspected lesion. The developed system can also allow the user to perform interactive operation for evaluation of lung lesions and structures through a user-friendly interface. These functions provide the user with powerful tools to observe and investigate clinically interesting regions through unconventional radiographic viewings and analyses. The developed functions can also be used to view and analyze patient's lung abnormalities in surgical planning applications. The system is currently under a clinical evaluation. Additionally, we see the possibility of using the system for teaching anatomy as well as pathology of the human lung.

(9) References

Ballard D.H., "Generalizing The Hough Transform to Detect Arbitrary Shapes," Pattern Recognition, vol. 13, No. 2, pp. 111~122, 1981.

Barr A.H., "Superquadrics and Angle-Preserving Transformations," IEEE Computer Graphics Applications, vol. 1, pp. 11-23, 1981.

Lo, S.C., Chan, H.P., Lin, J.S., Li, H., Freedman, M.T., and Mun, S.K., "Artificial Convolution Neural Network for Medical Image Pattern Recognition," Neural Networks, 1995, Vol. 8, No. 7/8, pp. 1201-1214.

Press W.H., Teukolsky S.A., Vetterling W.T., and Flannery B.P., "Numerical Recipes in C," Cambridge University Press, 1992.

Stitik F.P., Tockman M.S., and Khouri N.F.: Chest radiology. In Miller AB (ed.): Screening for Cancer, New York, Academic Press, 1985, 163-191.

Terzopoulos D. and Metaxas D., "Dynamic 3D Models with Local and Global Deformations: Deformable Superquadrics," IEEE Transactions on Pattern Analysis and Machine Intelligence, vol. 13, no. 7, pp. 703-714, 1991.

Zwirewich C.V., Vedal S., Miller R.R., Muller N.L. "Solitary Pulmonary Nodule: High-Resolution CT and Radiologic-Pathologic Correlation," Radiology, 1991; 179: 469-476.

Appendices:

(1) CT Images Display Functions for the Potential Improvement of Lung Cancer Diagnosis in The Developed Lung Cancer Detection System.

(2) Delegacz A., Lo S-C.B., Choi J.J., Xei H.C., Freedman M.T., and Mun S.K. "Three-Dimensional Visualization System as an Aid for Lung Cancer Diagnosis," SPIE Proc. Med. Imag., Vol. 3976, 2000, pp. 401-409.

(3) Delegacz A., Lo S-C.B., Freedman M.T., and Mun S.K. "Feature Extraction, Analysis, and 3D Visualization of Local Region in Volumetric CT Images," SPIE Proc. Med. Imag., Vol. 4319, 2001, pp. 76-81.

Appendix 1

CT Images Display Functions for the Potential Improvement of Lung Cancer Diagnosis

Description of Figures

Figure A1. System entry panel for the use of function tools designed for diagnosis of lung cancer
Only authorized users can login to the system with an eligible user name and password.

Figure A2 A pictorial index display for fast access to the slice of interest
The user can click the box of pictorial index to view the full-size CT slice.

Figure A3. Sequence view of 3 original CT slices.
The central slice is displayed in the top left corner. Bottom left and bottom right portion of the screen is used to present preceding and succeeding slices in the sequence respectively. Forward and rewind control buttons (not shown on the picture) are available for the user to choose the slices to be displayed from the whole sequence. A density color table is shown in the top right corner. It is a tool that can be used to display densities representing particular types of tissues (organs) in user-defined colors.
Remarks:
1) The density color table was not utilized when preparing this series of figures, therefore all the density entries in this and next figures are by default set to the value of 1.00.
2) In this and all following figures an arrow is used to point at a pulmonary nodule as an object of particular interest in applications of the 3D visualization system as an aid for lung cancer detection.

Figure A4. Image enhancement tools.
A standard set of tools is available to enhance the quality of displayed images. The figure shows a window width/level function tool in the bottom left corner as well as a brightness control tool in the bottom right corner of the screen. The top left portion of the screen displays the modified version of an original slice image.

Figure A5. Function tools for cutting arbitrary orientation in 3D.

The cutting tools presented in this figure allow the user interactive positioning of three available cutting planes in any chosen direction and orientation. The top left portion of the screen shows the three-dimensional simplified surface-rendered model of a body with the current location of cutting planes. Using the pointing device, the user can change the position and angle of each of cutting planes (independently of the others) with respect to the fixed body as well as rotate and move a body keeping the position of cutting planes frozen. The control diagram on the top right corner allows for precise specification of the cutting planes angles as well as other parameters (e.g. a zooming factor). The bottom left, middle, and right portions of the screen show the image contents of three cutting planes.

Figure A6. Three principal axes views

After setting the requested parameters for location and angles of cutting planes, the tools can be removed from the screen leaving the resulting images on screen.

Figure A7. Surface rendering of a section of thorax combined with a cutting plane view.

One of the advanced imaging techniques implemented in the 3D visualization system is surface rendering. It is used to depict the shape characteristics of a portion of the whole body or selected organs (e.g. lungs, bronchi, vessels). Combination of surface rendering and a cutting plane view as shown on this picture results in a valuable type of presentation allowing for seeing the spatial relationships among objects of interest (the pulmonary nodule) and surrounding tissues.

Figure A8. Combination of volume and surface rendering of a slab of thorax.

Volume rendering implemented in the 3D visualization system is one of the most advanced imaging techniques that allows for a very detailed and clear presentation of three-dimensional objects. The volume rendering technique gives a clear representation of locations, shapes and spatial relationships of objects or their portions. The built-in functions of the system, like rotating, panning or zooming allow for even deeper insight into the 3D characteristics of objects under consideration. The combination of powerful features of volume rendering with a surface rendering method results in a presentation view.

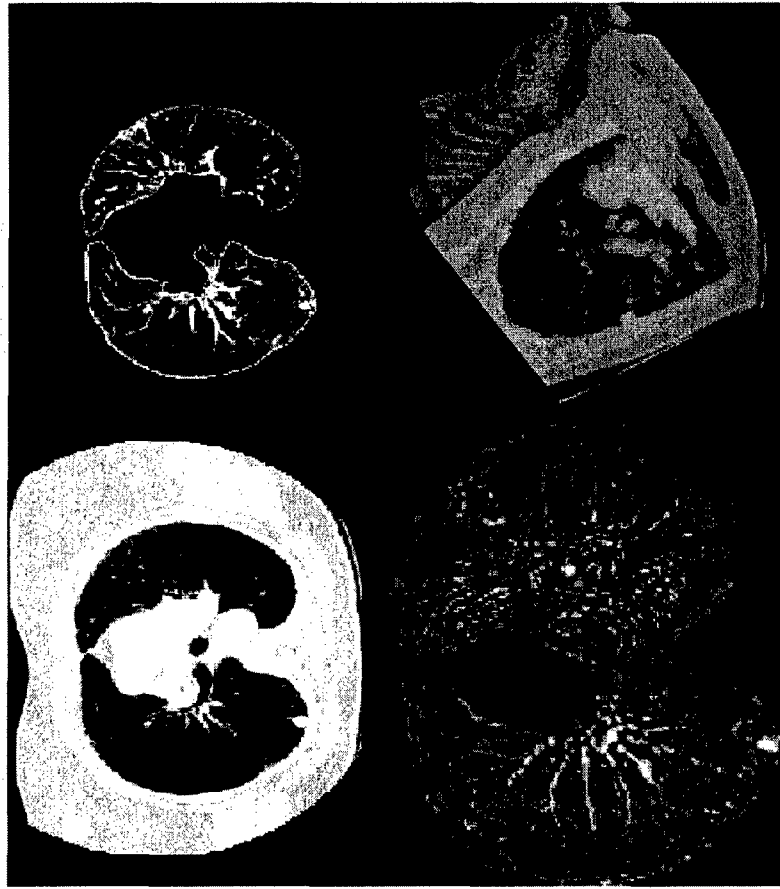Figure A9. Real-Time 3D presentation of rib cage and heart.

A volume rendering display is applied to the rib, heart, and other high intensity region. The rotation, panning, and zooming functions are come with the display function controlled by the mouse.

Figure A10. Contour of the lung object overlaid with an original slice image.
In Figures 3 to 9, the original unsegmented slices have been used to produce various types of presentation views. The system can accurately delineate lung region from the rest of chest structure. This figure shows that the contour of lungs as well as a nodule overlay on the original slice image.

Figure A11. Segmented lung area in 3 consecutive slices.
After finding the contour of the lung area, the next step in segmentation is to use it to extract the lung area from the original slice images. The figure shows the results of such extraction for the same original slices as shown in Figure 3.

Figure A12. Three principal axes views of lung only image
Similarly to the picture in Figure 6, the cutting planes images of segmented lung area can be presented on the screen without showing the tool controls.

Figure A13. Volume rendering of a section of segmented lung area.
The volume rendering technique as described earlier (see comments to Figures 6 and 7) is applied here to the segmented lung area. The details of the lung structures as well as a nodule can be clearly seen on this example picture.

Figure A14. Volume rendering of a section of segmented lung area – another example.

Figure A15. Real-Time 3D presentation of tumor vascularture.
A real-time 3D display function has also been developed to show a local volume of interest that allows the radiologist to inspect the tumor vasculature. Again, the rotation, panning, and zooming functions are come with the display function.

ISIS
Research
Center

Lung Cancer Detection Tools
LCDT

Password :

OK   Cancel

Figure A1. System entry panel for the use of function tools designed for diagnosis of lung cancer

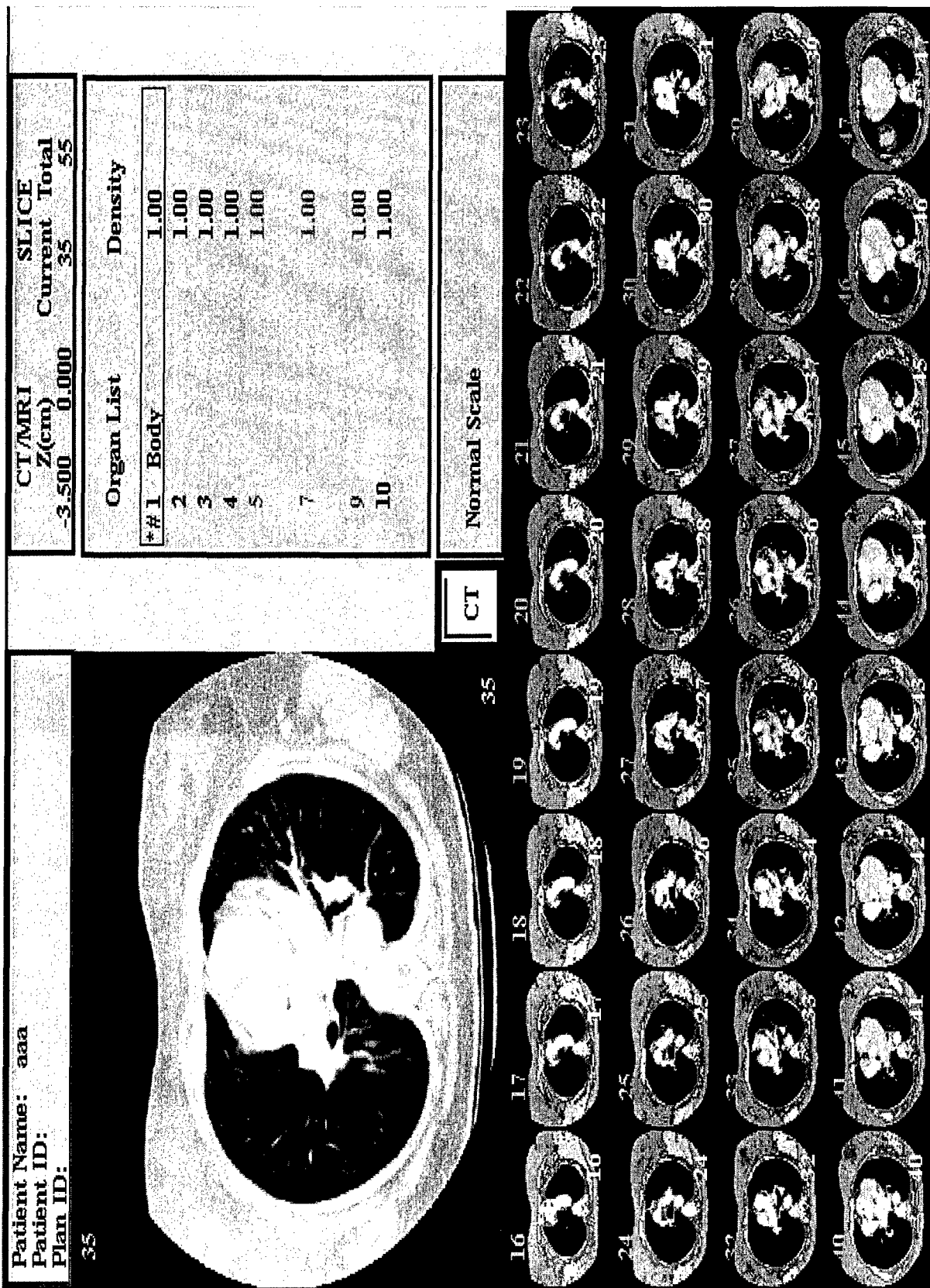CT Images Display Functions for the Potential Improvement of Lung Diagnosis
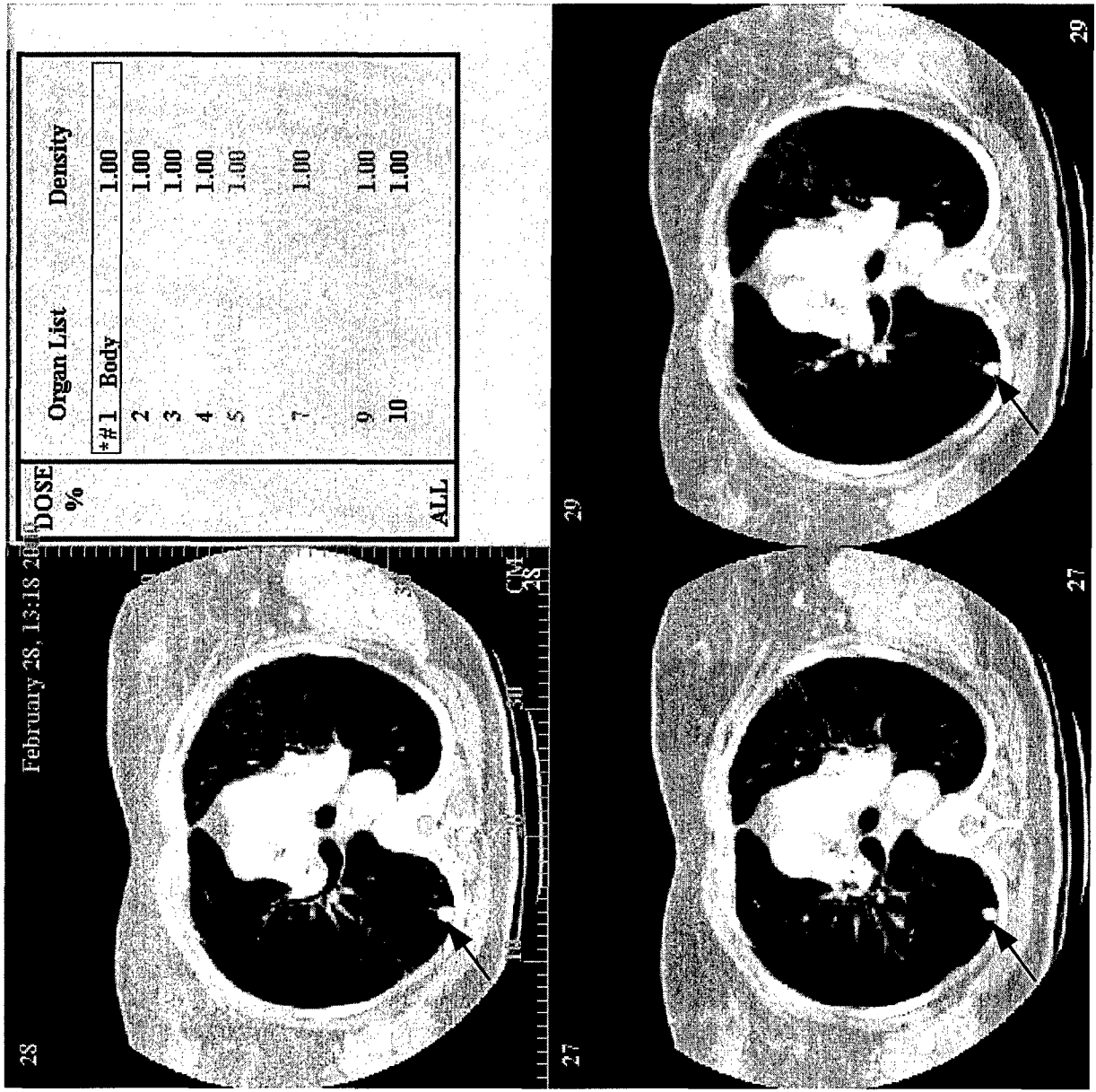
Figure A2. Pictorial Index for fast access to the slice of interest
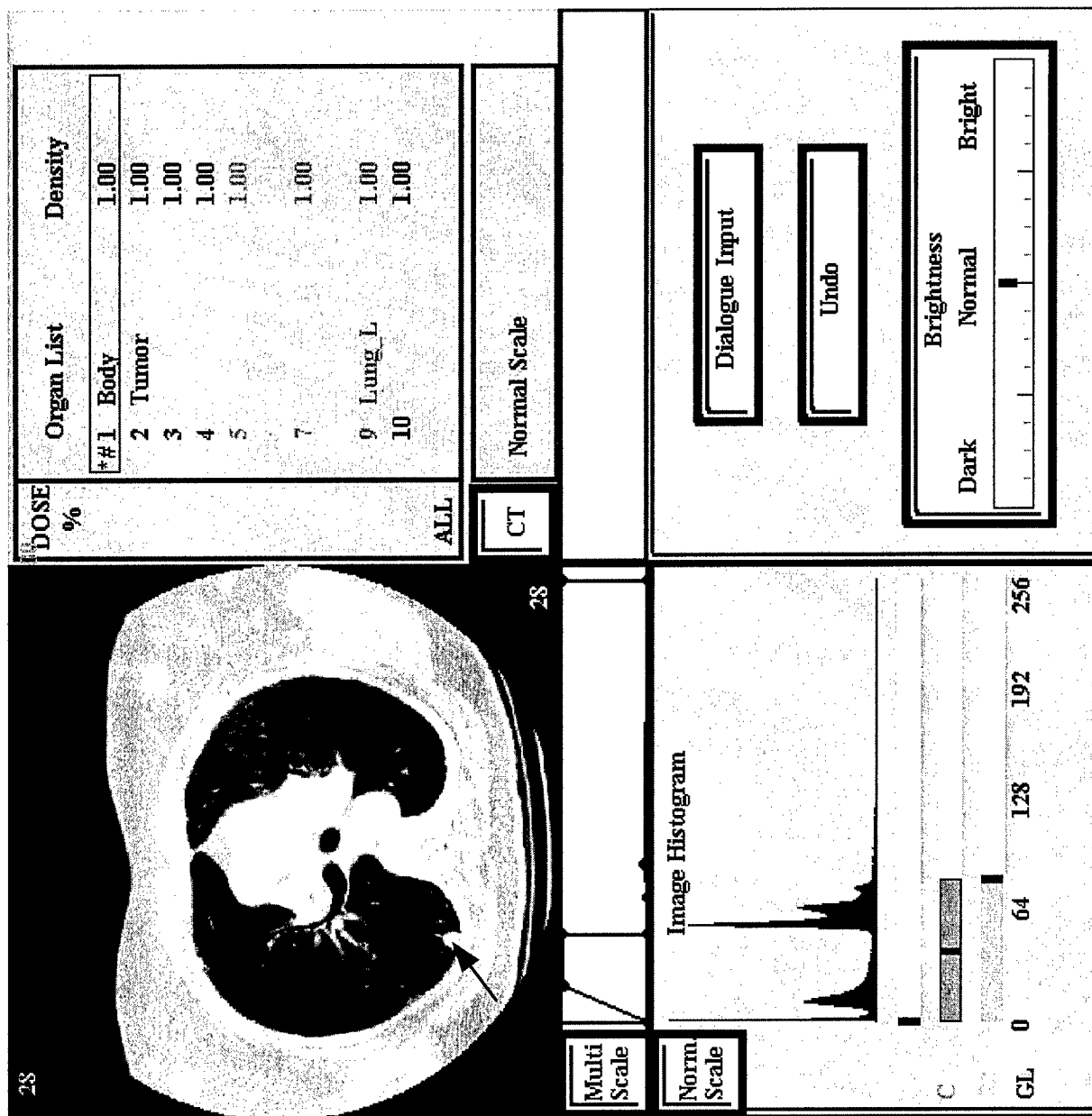
Figure A3. Sequence view of 3 original slices.

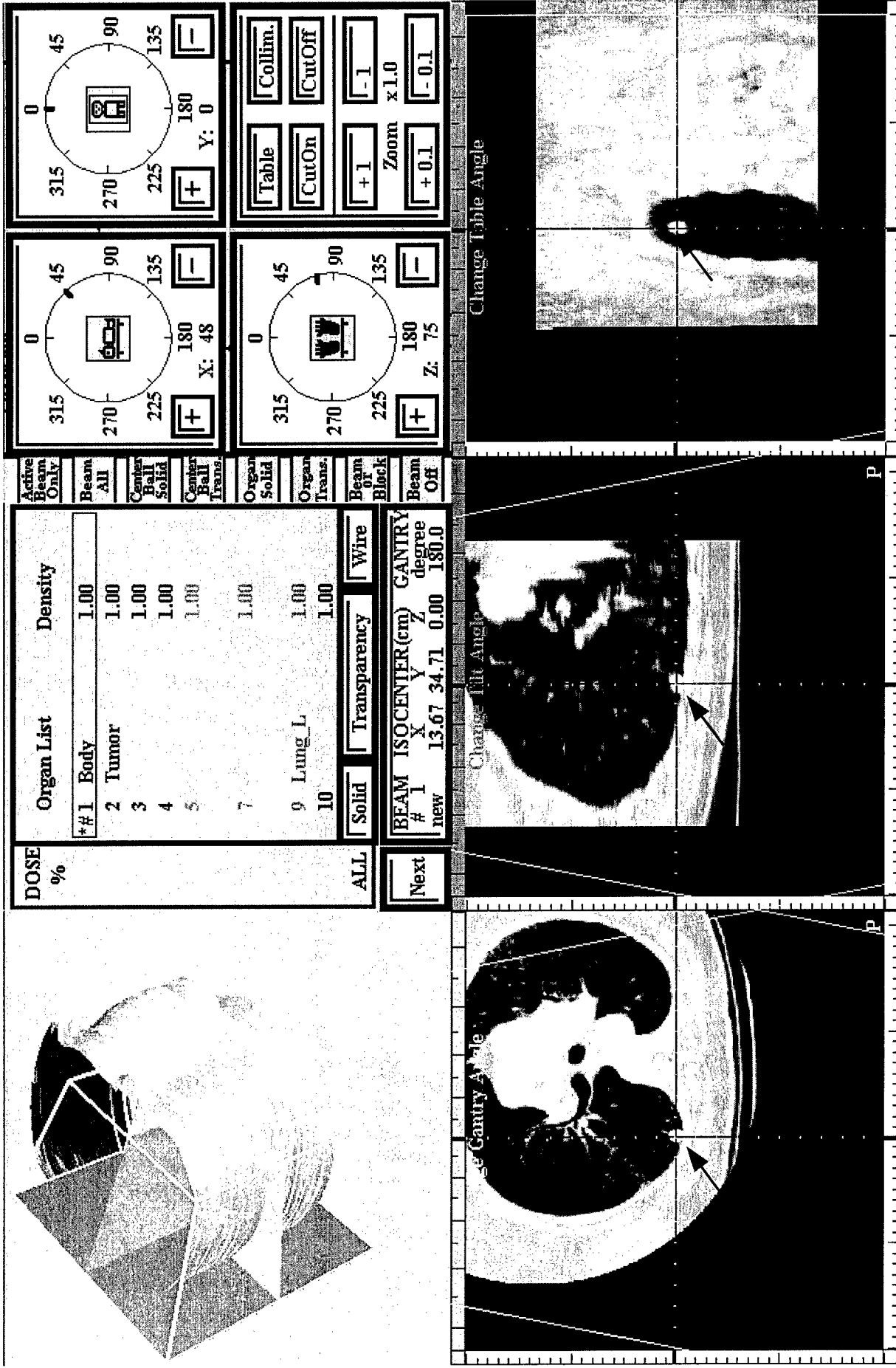Figure A4. Image enhancement tools using window/level functions.

Figure A5. Function tools for cutting 3D planes.

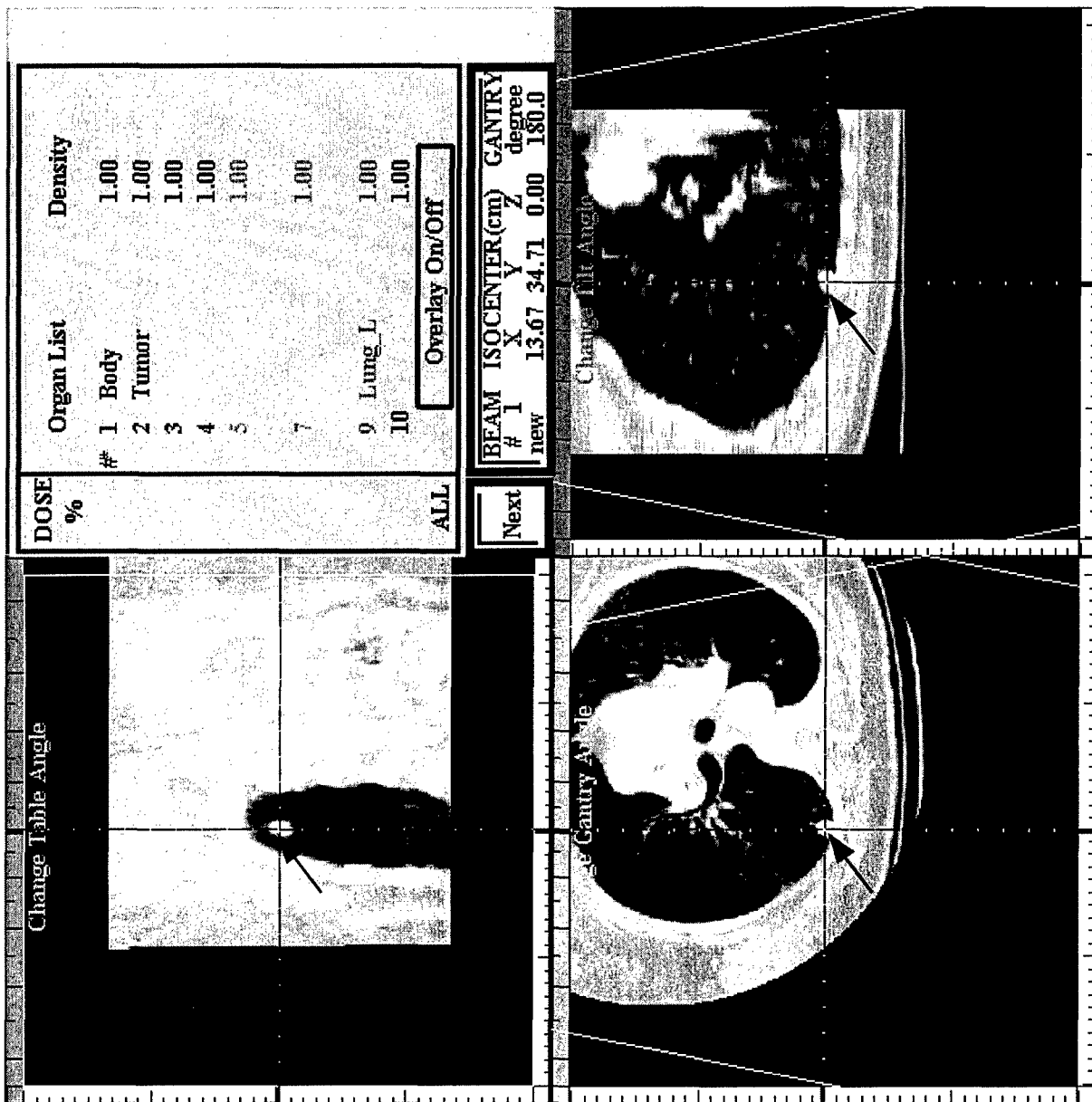CT Images Display Functions for the Potential Improvement of Lung Diagnosis
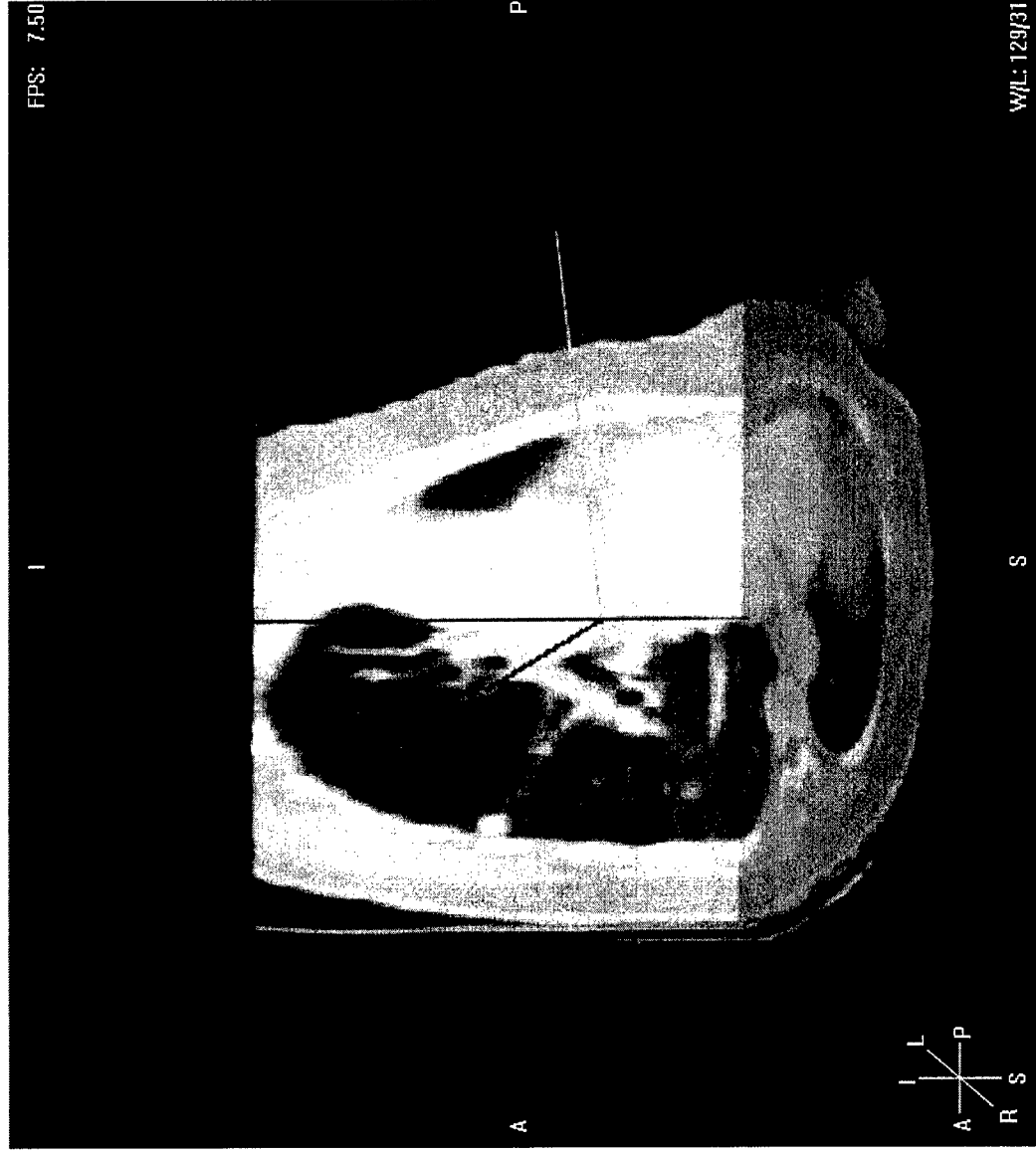
Figure A6. Three principal axes views.

Figure A7. Surface rendering of a section of thorax combined with a cutting plane view.

Figure A8. Combination of volume and surface rendering of a slab of thorax.
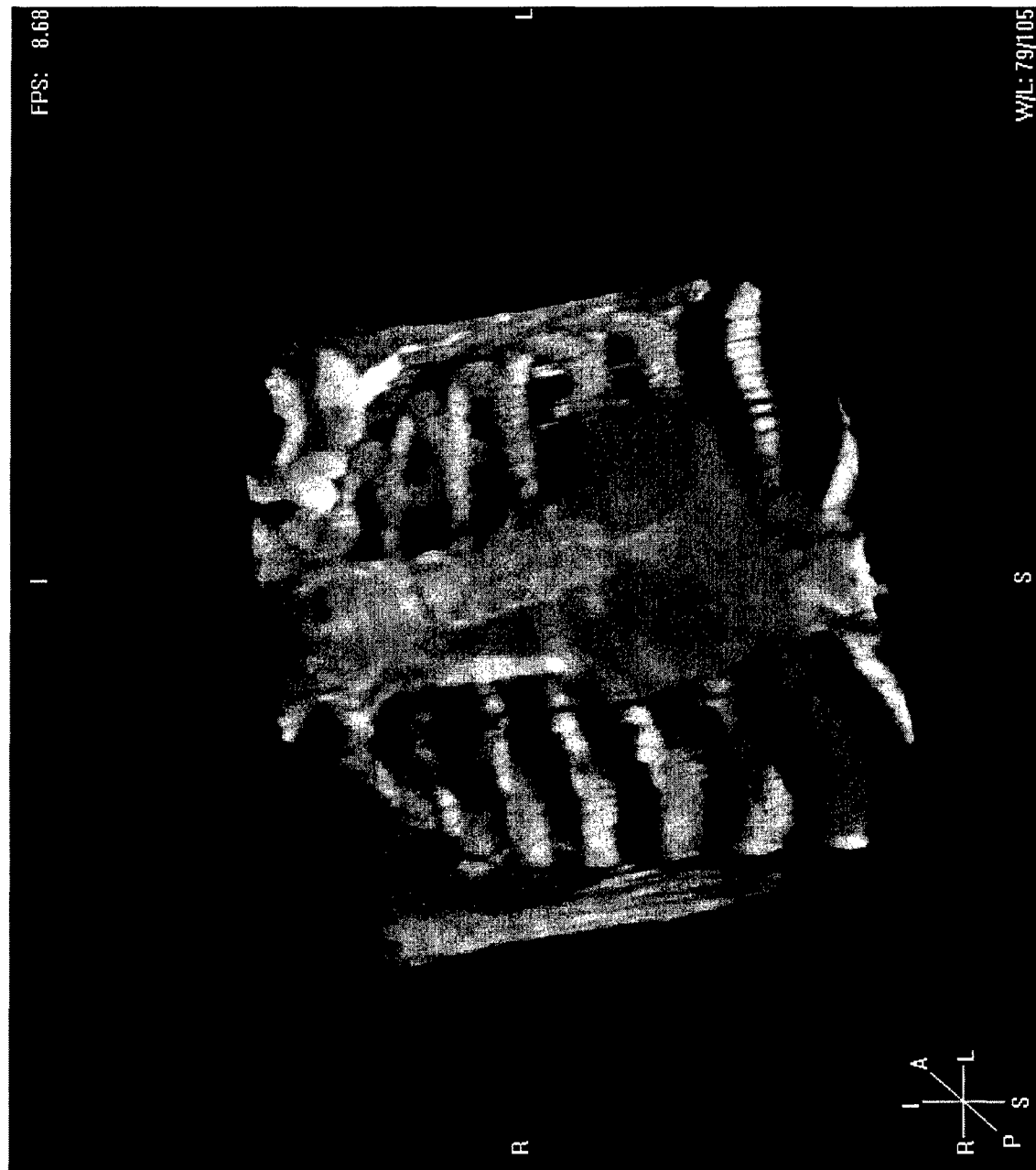
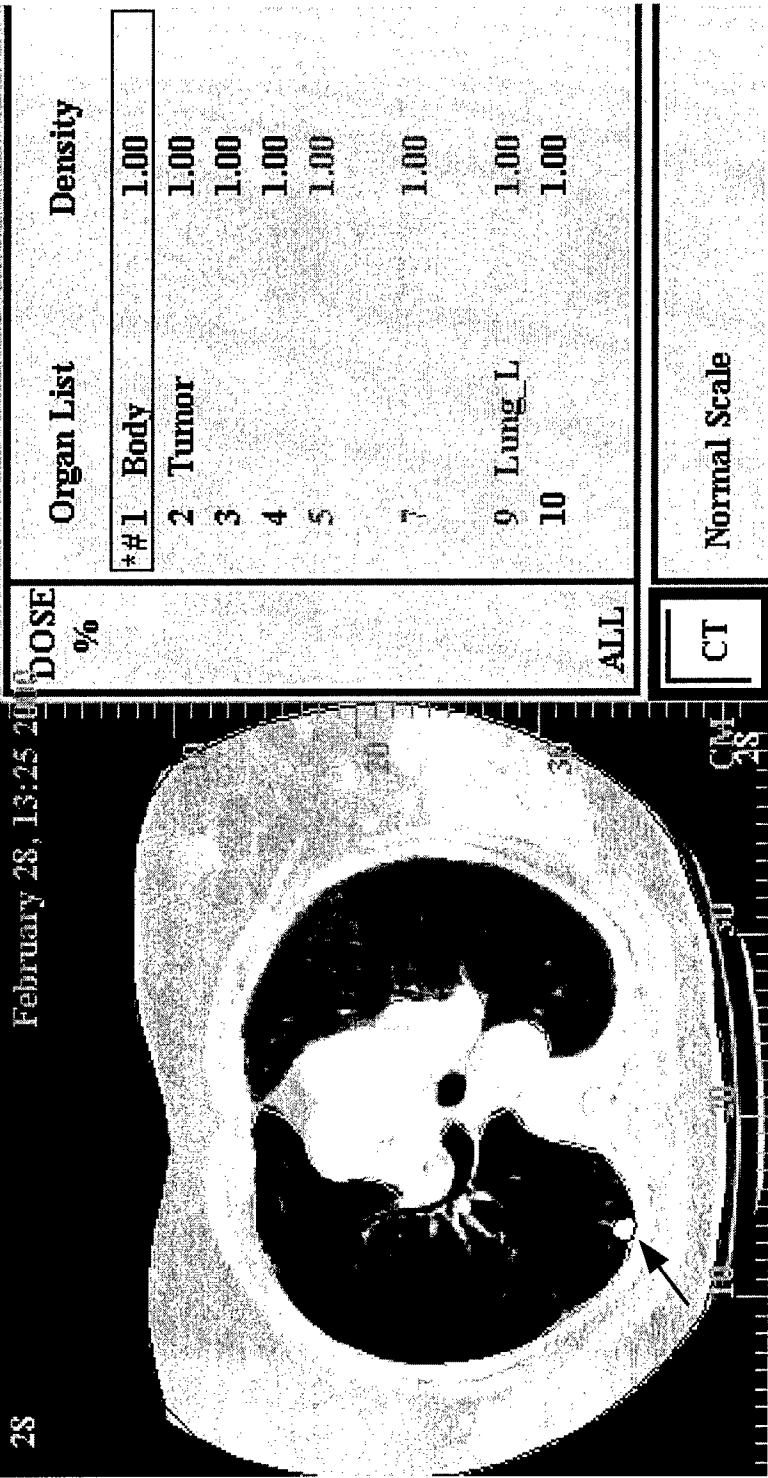Figure A9. Real-Time 3D presentation of rib cage and heart.

Figure A10. Contour of the lung object overlaid with an original slice image.

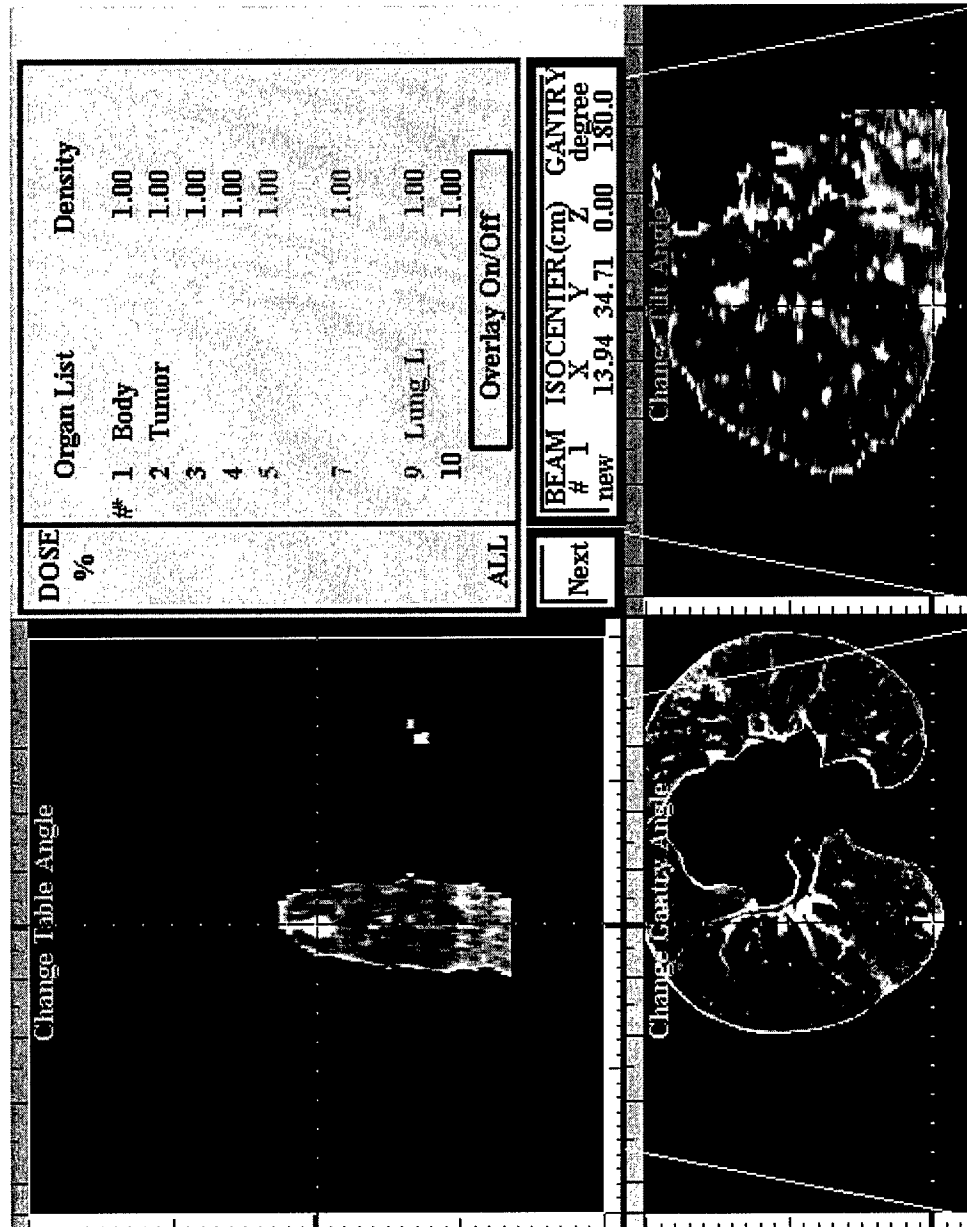Figure A11. Segmented lung area in 3 consecutive slices.

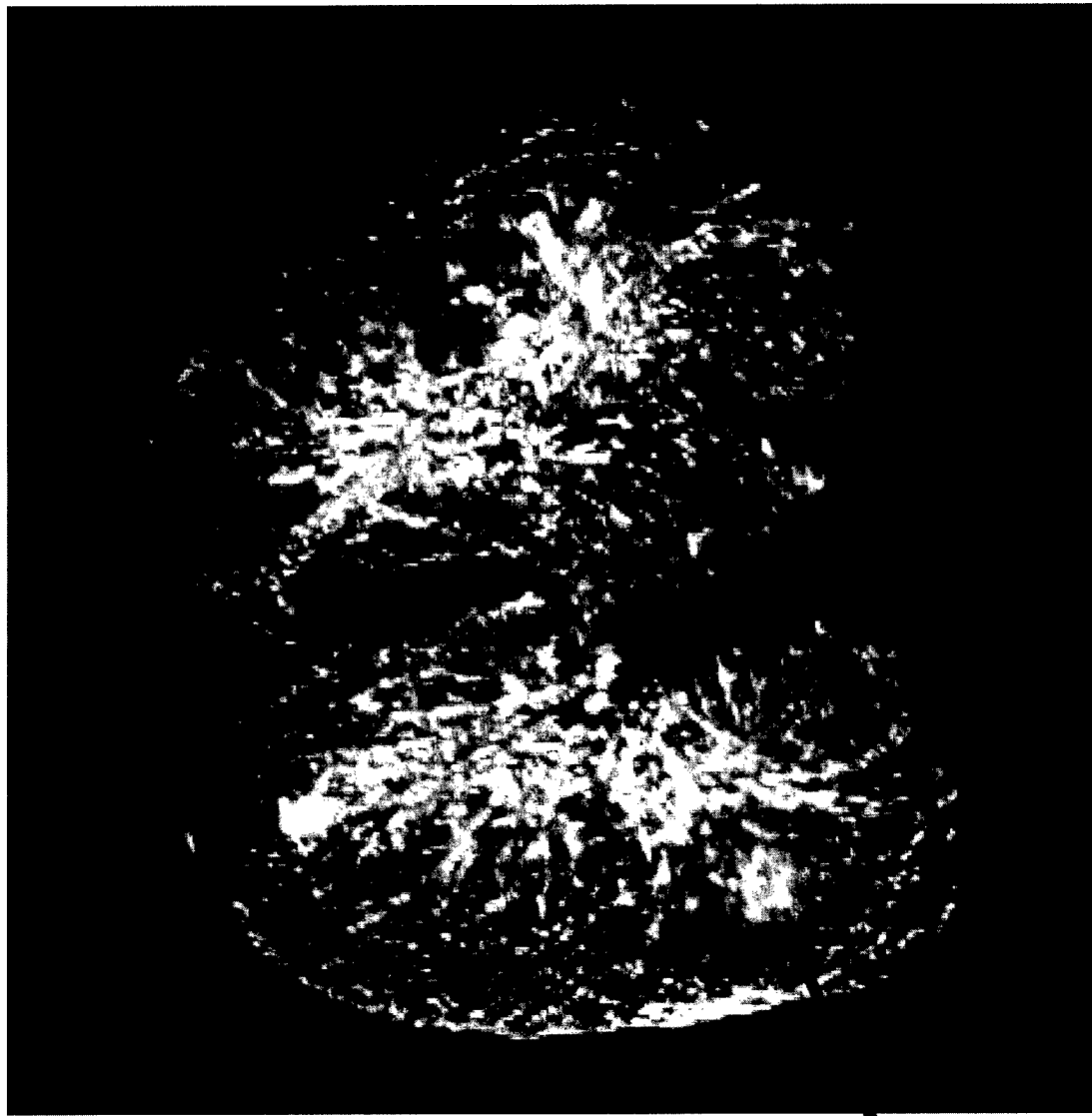Figure A12. Three principal axes views of lung only image

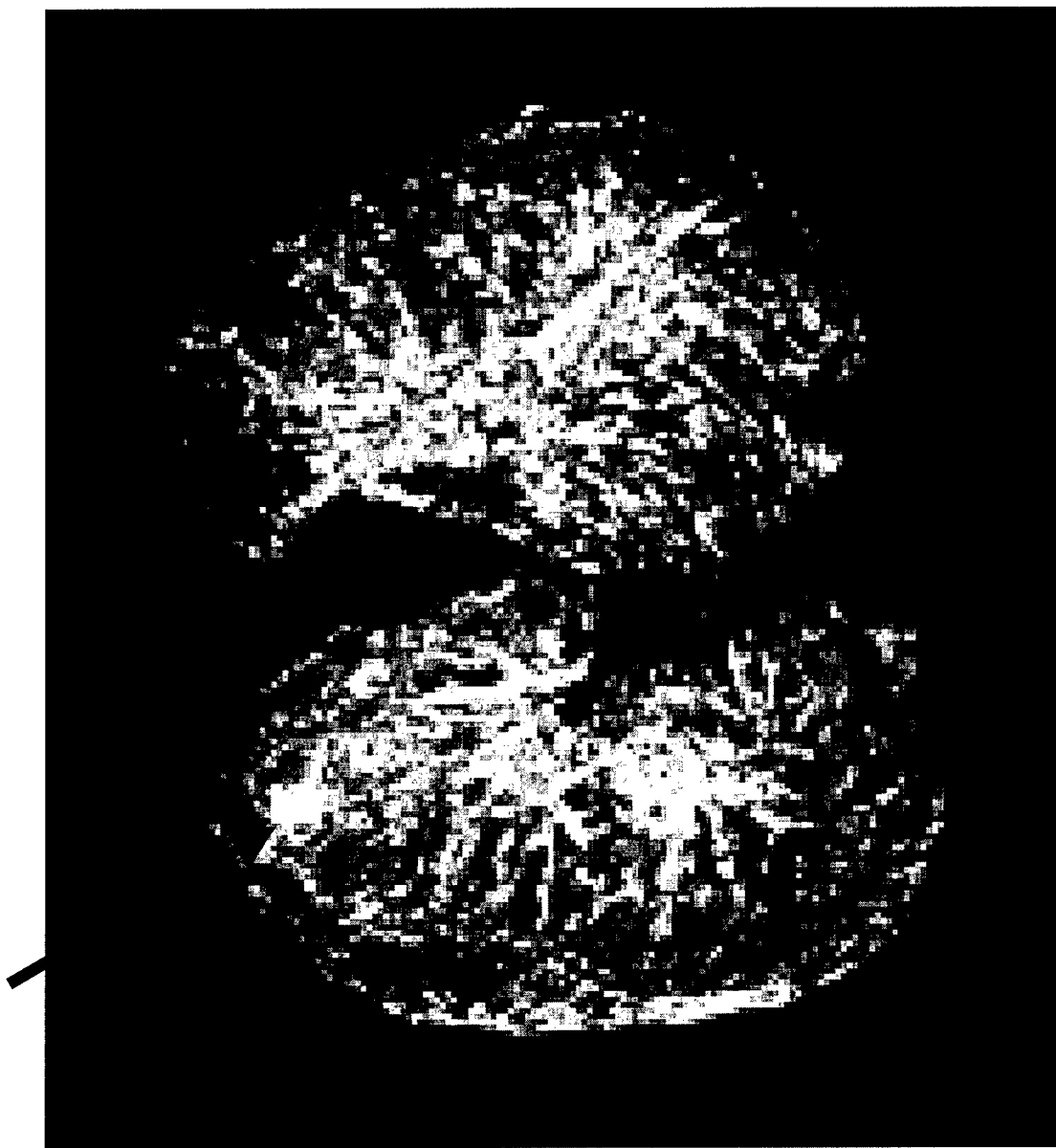Figure A13. Volume rendering of a slab of segmented lung area.

Figure A14. Volume rendering of a section of segmented lung area – another example.
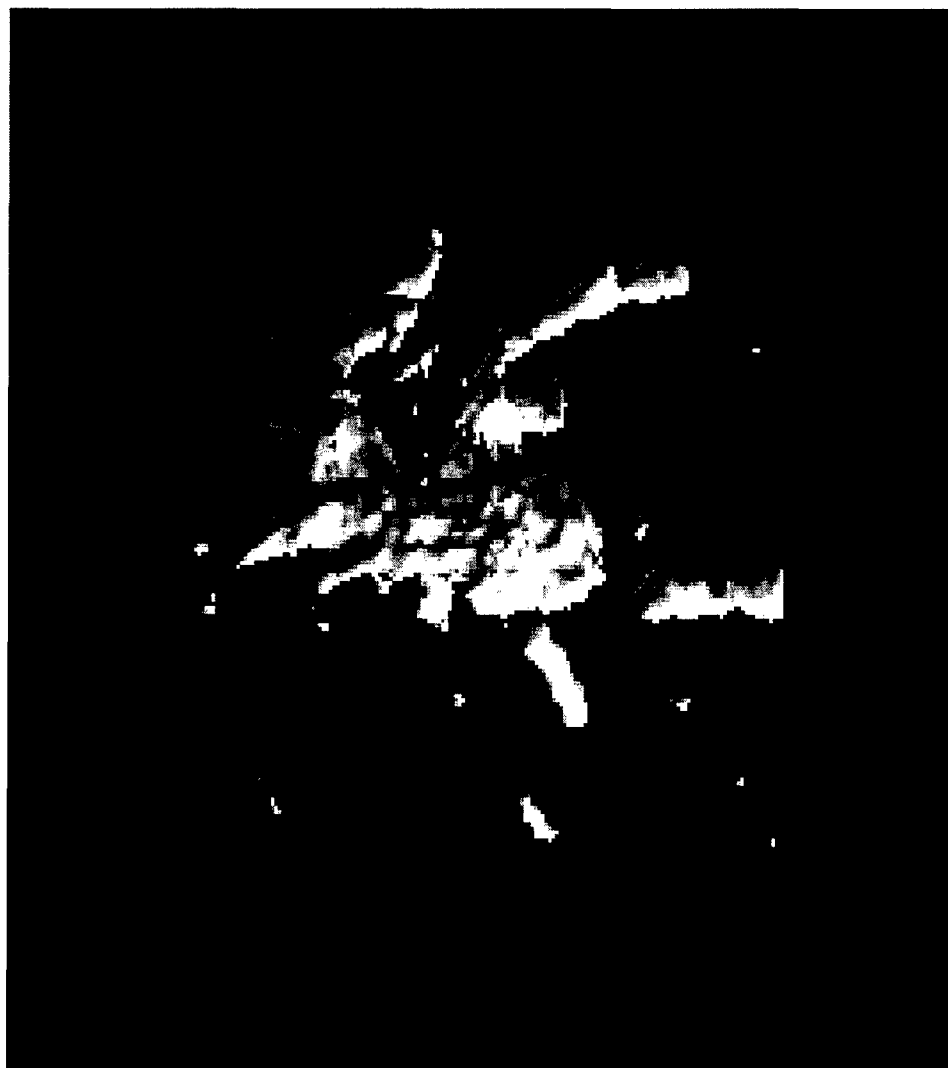
Figure A15. Real-Time 3D presentation of tumor vascularture.

Three-dimensional visualization system as an aid for lung cancer detection

Andrzej Delegacz[a,b], Shih-Chung B. Lo[a], Huchen Xie[c], Matthew T. Freedman[a], Jae J. Choi[d]

[a]ISIS Center, Georgetown University Medical Center, Washington, DC
[b]Department of Electrical Engineering, Catholic University of America, Washington, DC
[c]National Institute of Health, Bethesda, MD
[d]Department of Computer Science, Seoul National University, Seoul, Republic of Korea

ABSTRACT

The purpose of the work was to create a three-dimensional (3-D) visualization system to aid physicians in observing abnormalities of the human lungs. A series of 20-30 helical CT lung slice images (typical reconstruction interval: 6-10 mm) obtained from the lung cancer screening protocol as well as a series of 100-150 diagnostic helical CT lung slice images (typical reconstruction interval: 1-2 mm) were used as an input. We designed a segmentation filter to enhance the lung boundaries and filter out small and medium bronchi from the original images. The pairs of original and filtered images were further processed with the contour extraction method to segment out only the lung field for further study. In the next step the segmented lung images containing the small bronchi and lung textures were used to generate the volumetric dataset input for the three-dimensional visualization system. Additional processing for the extracted contour was used to smooth the 3-D lung contour in order to eliminate edge discontinuities related to bronchi as well as abnormalities (e.g. nodules) located close to the lung boundaries. The computer program developed allows, among others, viewing of the three-dimensional lung object from various angles, zooming in and out as well as selecting the regions of interest for further viewing. The density and gradient opacity tables are defined and used to manipulate the displayed contents of 3-D rendered images. Thus, an effective "see-through" technique is applied to the 3-D lung object for better visual access to the internal lung structures like bronchi and possible cancer masses. These and other features of the resulting 3-D lung visualization system give the user (physician) a powerful tool to observe and investigate the patient's lungs. The filter designed for this study is a completely new solution that greatly facilitates the boundary detection. The developed three-dimensional visualization system dedicated from chest CT provides the user a new way to explore effective diagnosis of potential lung abnormalities and cancer. In the authors' opinion, the developed system can be successfully used to view and analyze patient's lung CT images in a new powerful approach in both diagnosis and surgery-planning applications. Additionally, we see the possibility of using the system for teaching anatomy as well as pathology of the human lung.

Keywords: three-dimensional visualization, medical imaging, helical CT, image filtering, image segmentation, boundary detection, image processing, volume rendering, lung cancer detection

1. INTRODUCTION

It is known that early diagnosis plays an important role for most cancer cases including lung cancer allowing significantly better disease treatment outcomes as well as survival rates. Since the 1980s, rapid development and implementation of computer-aided detection and computer-aided diagnosis systems for various cancer detection and diagnosis have been observed in the field. In addition, more and more computer-based techniques are proposed to enhance diversified clinical applications in various cancer detection and/or diagnosis purposes. The choice of particular imaging modality depends on multiple factors such as the type of examined tissues (brain, lung, bones), the type of study (screening, diagnosis, functional study, surgery-assistance imaging), availability,

costs, etc. Furthermore a rapid growth of research is seen in the field of image fusion in combining the best characteristics of two or more medical imaging modalities to create a new avenue in diagnostic imaging.

In the particular area of lung imaging aimed to support screening and diagnosis of lung diseases the radiographic methods like conventional X-ray (XR) and computed tomography (CT) are most commonly used. Recently the low-dose helical (spiral) CT scanners are growing in popularity due to the high resolution and superb quality of images. Usually, tomography devices generate a substantial amount of data for a single examination. Therefore it is more difficult for radiologists to review and analyze the examination with conventional methods. This leads to an emerging need for visualization techniques that combine and process the original images giving users the tools for faster, more efficient diagnosis. Moreover, the high spatial resolution in the z-axis and the corresponding large number of slices allow the construction of a volumetric dataset that can be used as an input to 3-D visualization systems by applying surface and/or volume rendering techniques.

2. OVERVIEW OF 3-D VISUALIZATION TECHNIQUES FOR CT LUNG IMAGES

A large spectrum of visualization techniques has been developed to overcome the two-dimensional constraints of imaging modalities and to support better insight into the human body[1,2]. Some of those techniques employ the 2-D paradigm, however, introducing the mechanisms to manipulate and present 2-D images in a particular way, can significantly enhance the user's ability to understand the overall 3-D picture. The typical example of such a technique is a "slice sequence" of 2-D CT images. Single CT image frames can be processed (e.g. with the use of lesion detection algorithms) and/or displayed either forth and back (or with the loop) one frame at a time or as a sequence of consecutive frames in parallel. This method takes one image at a time and lends itself to an easy but rapid way to review the full CT scan. In addition, a zoom capability enables the user to recognize and further process the regions of interest. The "slice sequence" technique is widely used in clinical practice and is commercially available.

A stack of images converted into a 3-D regular or irregular data grid is most often used as an input for 3-D rendering methods. Before submission to the 3-D visualization system the input data is usually preprocessed with segmentation algorithms to select the objects of interest. The final result is either the 3-D surface or volumetric representation of the acquired dataset.

Most well known surface rendering techniques utilize various types of triangulation algorithms to create the 3-D mesh as a basis for the construction of the 3-D surface itself. The shading and coloring algorithms are further used to improve the quality, readability and accuracy of the resulting image. 3-D surface rendering is a valuable tool to reconstruct the contours of the objects, thus presenting their shapes, location and spatial relationships. However, by its nature, surface rendering does not allow visualizing the "contents" of hidden objects. For this purpose a volume rendering technique has to be employed.

In contrast to surface rendering, volume rendering algorithms operate directly on volumetric data to produce an image without generating an intermediate geometric representation. This approach gives greater flexibility in visualizing internal structures without the necessity to define their contours. As such it is ideal to be used in medical imaging applications. The two basic volume rendering classes of algorithms – image-order and object-order methods - are well known and widely used. Furthermore, hybrid algorithms have been developed that combine the pure image- and object-order approaches to take advantage of their best characteristics and result in improved quality as well as greater rendering speed. An example hybrid technique is a shear-warp factorization algorithm developed by P. Lacroute and M. Levoy[8] that was employed in our system described below.

3. PRE-PROCESSING OF THE DATA FOR CT LUNG IMAGES

Each of the previously mentioned visualization techniques has its scope of application and essentially cannot be replaced with the others. For the 3-D visualization system to be complete it is necessary to incorporate all those techniques in one package. This idea was the authors' goal when creating a 3-D visualization system to aid in lung cancer detection. We built a system that makes use of the "slice sequence" view, 3-D surface and volume rendering as well as sliding thin slab view techniques to provide the user with a comprehensive set of tools to facilitate effective inspection and detection of suspicious lung regions.

3.1. Input Data

As the standard input data we used the helical CT screening and diagnostic scans of human lungs. Screening CT scans consisted of 20-30 slices with a reconstruction interval of 6 mm. In diagnostic CT scans the number of slices was 100-150 with a reconstruction interval of 2 mm. For both types of CT scans the resolution of a single slice was 512×512 pixels and the gray-level depth was 12 bits per pixel.

3.2. Resampling

For the purpose of better rendering rates on the PC computers without specialized graphics-acceleration hardware we chose to reduce the slice resolution to 256×256 pixels and gray-level depth to 8 bits. The bilinear interpolation method was used to resample the original slice images. Thus we could achieve the average rate of single frame rendering on the order of 0.5 second.

3.3. Interpolation between slices

Although the helical CT scanners produce a large number of slice images along the z-axis of the body, this number, representing the z-axis resolution, is still significantly smaller then the resolution in the slice plane (x-y axes). The z-axis resolution takes the value of about 30 for screening, and 120 for diagnostic scans, whereas the resolution of x- and y-axis is usually 512×512 pixels. To compensate for this discrepancy it is necessary to artificially increase the z-axis resolution to make it comparable to the x- and y-axes. One of the commonly used methods is to generate intermediate slices, which are inserted between the original ones from which they have been created. The number of intermediate slices generated depends on the original volume resolution. Ideally, the resultant z-axis resolution should be equal or close to the x- and y-axes resolutions. This would allow obtaining a "cubic" volume dataset maintaining the proper spatial proportions of the examined object. In practice, the z-axis resolution after the slice interpolation is usually chosen to be smaller and on the order of one-half to two-third the x- and y-axes resolutions. Various techniques can be applied to interpolate the intermediate slices. The classical linear interpolation and image warping techniques are the most popular[3,4,5]. For the purpose of our system development, we used the linear interpolation method creating 5-8 intermediate slices between each pair of original ones for screening CT scans, and 1-2 intermediate slices for diagnostic CT scans.

4. SEGMENTATION

To eliminate all tissues other then the lung tissue, we segmented the input CT images with the use of a segmentation filter and contour extraction procedure. The filter was especially designed to significantly differentiate between the lung tissue and all other body tissues. It was initially designed for the segmentation of X-ray chest films and used to process more than 500 cases with outstanding results[6]. It was further modified for this application to process CT chest images and utilized in this study to perform fully automatic segmentation. The very valuable characteristic of the designed filter is its capability to precisely select the lung field even if it contains very bright (high opacity) regions located on the boundaries of the lung field. An example of this situation is depicted in Figures 1 and 2.
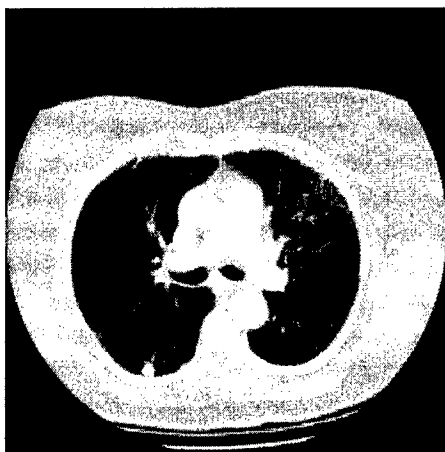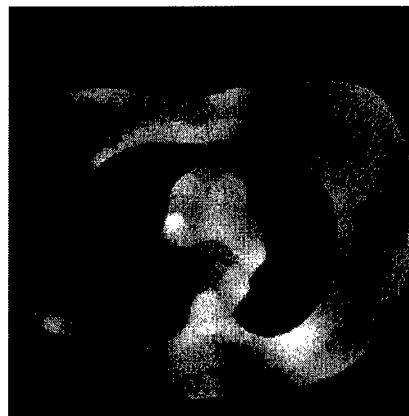
Figure 1. Original image.

Figure 2. Filtered image.

The next step of segmentation was to find the contours of the lung field from the slices processed with the segmentation filter. We used the contour tracking method for this purpose[7]. We observed that sometimes the contours of the lung field obtained with use of the filter covered an area slightly larger than actual lung field. To account for this artifact, we chose to apply the contouring algorithm more than once (usually 3-5 times) in a sequential order where the input slice to the contouring procedure in the current run was the output from the previous run (except the first run). In the last step of the segmentation, we used the last version of the contour as a template to extract the lung field on the original CT image. Figure 3 shows the whole segmentation path for a single slice.
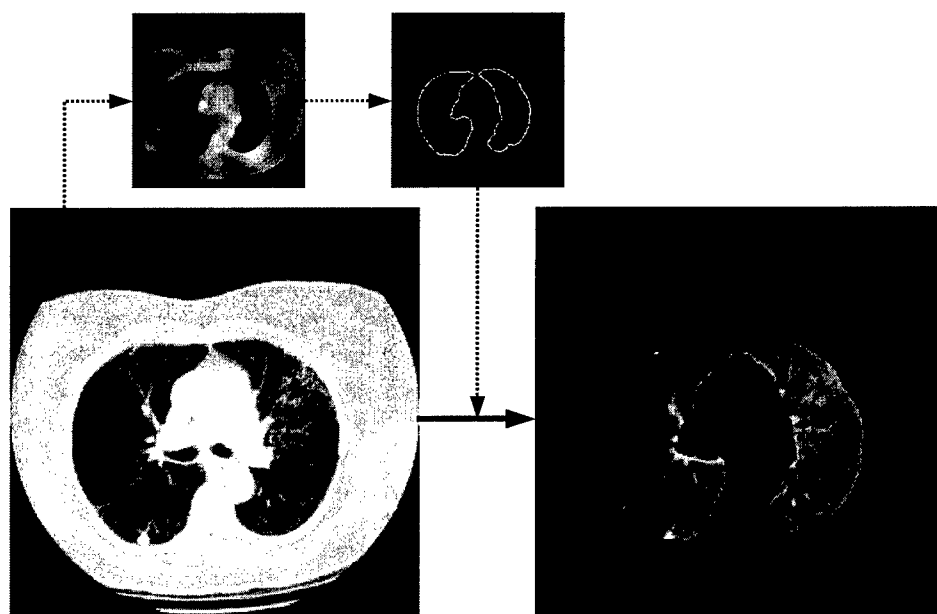

Figure 3. A diagram shows segmentation steps. (Bottom left: original image; Upper left: filtered image; Upper right: contour of the lung field delineated from the filtered image; Bottom right: extracted lung field.)

Finally the whole sequence of segmented CT slices was combined into one volume file that was then used as the input to the 3-D visualization system. The overall process of volume dataset preparation can be described in an algorithmic way by the following pseudo-code:

```
for each original_slice
        resampled_slice = resample(original_slice);

for each resampled_slice
{
        generate_intermediate_slices(resampled_slice, next_resampled_slice);
        insert_intermediate_slices(resampled_slice, next_resampled_slice);
}

for each interpolated_slice
{
        apply_segmentation_filter(interpolated_slice);
        contour_image = find_contour(interpolated_slice);
        for (index=1 to 3) do contour_image = find_contour(contour_image);
        segmented_slice = extract_lung_field(interpolated_slice, contour_image);
}

for each segmented_slice
        add_to_volume(segmented_slice);
```

5. 3-D VISUALIZATION SYSTEM FOR CT LUNG IMAGES

5.1. Slice sequence view

As mentioned in the overview section, the well known and popular slice sequence presentation of consecutive CT image frames is a useful tool to quickly review a whole or part of a volume dataset as well as to study the selected slices. We implemented this technique in a classical way. The user interface allows, among others, to change the size of displayed slices (thus changing the number of slices shown on the screen at the given time), forward and rewind the sequence, and move to the beginning and end of the sequence. The user can choose to see the full set of slices including the intermediate ones or the collection of original slices only. Several basic image functions are available for modification of image characteristics. (e.g. brightness, contrast, window width/level, and inverse image). Figure 4 shows an example of the slice sequence view.

Figure 4. An example of slice sequences that is typically shown on a 1Kx1K monitor.

5.2. Volume rendering

In this work, we intended to explore advanced applications of volume rendering as a tool to visualize the lung object structures. The volume rendering method used in this module is based on the shear-warp factorization algorithm by Philippe Lacroutte and Mark Levoy[8]. In particular, we utilize the VolPack volume rendering library, which implements the above mentioned algorithm. For the purpose of the project we ported the VolPack library to the PC/Windows environment. The library has been used to develop the interactive software module that allows for an in-depth inspection and analysis of the lung object in three dimensions. Among others, the software implements the following functions:

- performing the geometric transformations of the lung object: rotate, move, zoom in and out;
- modification of the transparency/opacity characteristics of the tissues comprising the lung object;
- projection of the lung object onto the cut plane at any angle;
- changing the lighting characteristics of the lung object and surrounding environment;
- changing the resolution of the rendered images;
- saving the single rendered frame to a disk file;
- saving the sequence of the rendered frames to a disk file.

The feature of altering the transparency/opacity characteristics is of particular value for efficient lung object viewing. An opacity array is used to translate the lung object original densities into the density opacity levels. Similarly the gradient values calculated in the pre-processing stage are related to gradient opacity levels through an appropriate array. The system allows for changing the individual opacity levels of each of 255 density and gradient values as well as constructing the opacity ramp based on few designated opacity levels. This approach gives full flexibility in modifying original densities and gradients of tissues comprising the lung object. Figures 5 and 6 present examples of images rendered by the system. The image shown in Figure 5 was rendered with opacity window level: 170, width: 128, and gradient window level: 12, width: 16. For rendering the image in Figure 6, we used opacity window level: 128, width: 64, and gradient window level: 8, width: 64. [Note: HU $\approx$ (8-bit value $\times$ 16) - 2000].
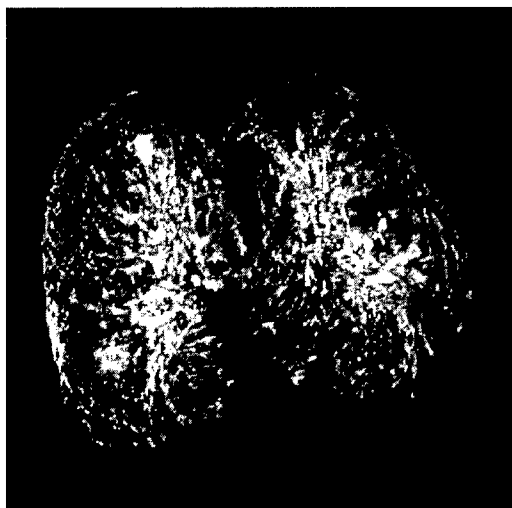

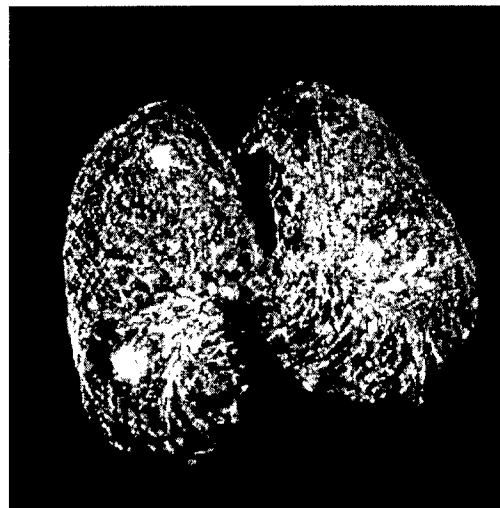Figure 5. Volume rendering of the lung (example 1).

Figure 6. Volume rendering of the lung (example 2).

5.3. Sliding thin slab

The volume rendering of the whole lung object provides some detailed information of the shapes, location, and spatial relationships of internal structures. The geometric transformations further increase the capability of seeing the details of the structures of interest. However, the inherent characteristic of this type of presentation is that

some internal structures obscure the other ones, thus making it difficult to see the details of the objects of particular interest, like nodules. For this purpose, we use the sliding thin slab (STS) projection[9,10,11], which overcomes the above mentioned difficulties. In our STS view the user is able to define the position, thickness, and size of the slab. The slab can be moved along the z-axis, and after fixing its position with respect to that axis; it can be further transformed with the use of the same functions as in rendering the whole lung object. Examples of the thin slab view projection are show in Figures 7 and 8.
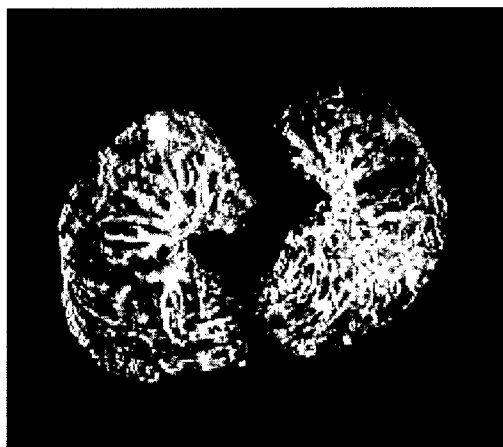

Figure 7. Sliding thin slab (thickness: 20 mm).
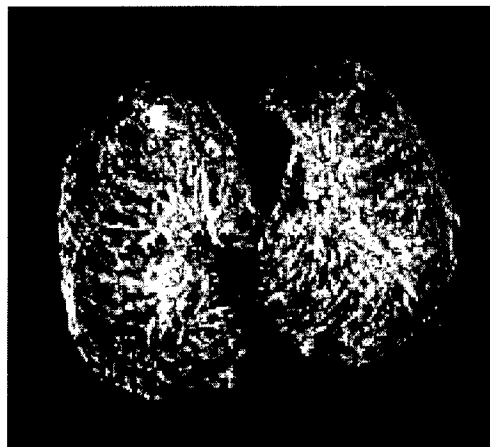

Figure 8. Sliding thin slab (thickness: 40 mm).

5.4. Surface rendering

Surface rendering, although in general not useful for visualizing internal structures, also finds limited clinical application for the visualization of lung nodules in CT images. We implement this technique to present the general look of the lung object - its shape and orientation in the 3-D coordinate system as well as the location and orientation of the cut planes utilized in other view modes. This view provides the means to rotate the lung object around all three axes and positioning the cut planes as desired by the user. Our design also allows for combining surface rendering with other views (slice sequence, volume rendering and sliding thin slab). The implementation of surface rendering was based on the marching cubes algorithm (Lorenson, Cline, 1987)[12]. Figure 9 shows an example of combined slice sequence and surface rendering modes applied to defining the sliding thin slab parameters. In Figure 10, we present the combination of surface and volume rendering used to specify the cut planes.

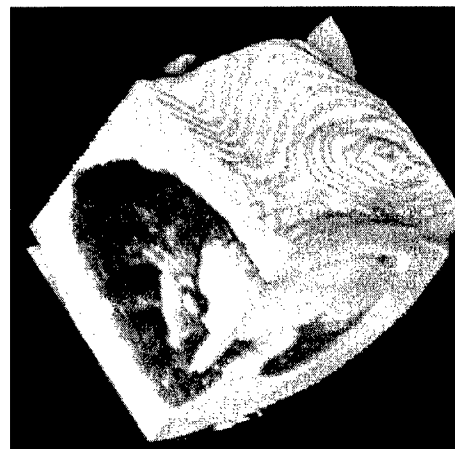Figure 9. Surface rendering and slice sequence view.

Figure 10. Surface and volume rendering example.

6. DISCUSSION

As mentioned earlier, 2-D "slice sequence" is the standard viewing method for screening CT images in current clinical practice. 3-D display, even with interpolation of slices, can only provide fuzzy structures without much image details. With the availability of a computer-aided detection algorithm in the viewing system, suspected areas can be highlighted in either 3-D or 2-D display to provide the radiologist with rapid and clear 3-D geometrical information for the evaluation of suspected lung nodules. Based on the computer-aided system development in this area so far, visual evaluation is necessary to determine clinically significant detections among those detected and undetected by the computer.

Diagnostic viewing requires a high-resolution CT scan with or without a contrast agent[13]. With regard to the diagnosis of solitary pulmonary nodules[14], specific features to assess the nodules on CT images include: (1) size and location, (2) margins and boundaries, (3) vessels and bronchi, (4) cavitation, (5) satellite nodules, and (6) density. 3-D and sliding slab view with advanced image processing techniques (e.g. enhanced bronchi, arteries, and veins[15]) will assist the radiologist in analysis of the characteristics of tumor margins, its association with vessels and bronchi, the wall thickness of tumor cavitation[16], and density level and uniformity of the tumor.

We believe, therefore, that the proposed viewing methods will be of great value for (1) rapid viewing in screening CT while cooperating with a computer-aided detection system and (2) enhancing clinical capability in assessing the property of the tumor while cooperating with a computer-aided diagnosis system. The purposes of this work were to (a) explore clinically useful display methods for viewing and diagnosis of lung images of CT, (b) establish an advanced display workstation for clinical evaluation, and (c) form a technical base to facilitate the development of computer-aided systems.

7. CONCLUSIONS

The segmentation filter designed for this study is a completely new solution that greatly facilitates the boundary detection. The developed three-dimensional visualization system gives the user a unique new way to conduct effective diagnosis of potential lung abnormalities and cancer. In authors' opinion, the developed system can be successfully used to view and analyze patient's lung CT images in a new powerful way in both diagnosis and surgery-planning applications. Additionally, we see the possibility of using the system for teaching anatomy as well as pathology of the human lung.

8. ACKNOWLEDGEMENTS

9. REFERENCES

1. P. S. Calhoun, B. S. Kuszyk, D. G. Heath, J. C. Carley, and E. K. Fishman, "Three-dimensional Volume Rendering of Spiral CT Data: Theory and Method," *RadioGraphics*, **19**, pp. 745-764, 1999.
2. J. K. Udupa, "Three-dimensional Visualization and Analysis Methodologies: A Current Perspective," *RadioGraphics*, **19**, pp. 783-806, 1999.
3. D. Ruprecht, and H. Muller, "Deformed Cross-Dissolves for Image Interpolation in Scientific Visualization," *Journal of Visualization and Computer Animation*, **5**(3), pp. 167-181, 1994.

4. D. Ruprecht, and H. Muller, "Image Warping with Scattered Data Interpolation Methods," *Research Report 443*, Fachbereich Informatik der Universitat Dortmund, Dortmund, Germany, 1992.
5. G. Wolberg, *Digital Image Warping*, IEEE Computer Society Press, Los Alamitos, California, 1990.
6. S. Lo, and H. Zhao, "Filter Based Image Segmentation: Application to Lung Field Extraction in Chest Radiography," submitted to *IEEE Tran. On Medical Imaging*.
7. D. Watson, *Contouring: A Guide to the Analysis and Display of Spatial Data*, Pergamon Press, New York, 1992.
8. P. Lacroute, and M. Levoy, "Fast Volume Rendering Using a Shear-Warp Factorization of the Viewing Transformation," in *Computer Graphics (SIGGRAPH '94 Proceedings)*, pp. 451-458, Orlando, Florida, 1994.
9. S. Napel, G. Rubin, and R. B. Jeffrey, Jr., "STS-MIP: A New Reconstruction Technique for CT of the Chest," *Journal of Computer Assisted Tomography*, 17(5), pp. 832-838, 1993.
10. S. Y. Yen, G. Rubin, and S. Napel, "Fast Sliding Thin Slab Volume Visualization," in *Proceedings of the 1996 Symposium on Volume Visualization*, pp. 79-86, San Francisco, California, 1996.
11. S. Y. Yen, G. Rubin, and S. Napel, "Fast Sliding Thin Slab Visualization of CT and MR Angiograms," *RSNA EJ*, 1, 1997.
12. W. E. Lorensen, and H. E. Cline, "Marching Cubes: A High Resolution 3D Surface Construction Algorithm," *Computer Graphics*, 21(4), pp. 163-169, 1987.
13. S. J. Swensen, L. R. Brown, T. V. Colby et al., "Lung Nodule Enhancement at CT: Perspective Findings," *Radiology*, 201(2), pp. 447-455, 1996.
14. C. V. Zwirewich, S. Vedal, R. R. Miller, and N. L. Muller, "Solitary Pulmonary Nodule: High-Resolution CT and Radiologic-Pathologic Correlation," *Radiology*, 179(2), pp. 469-476, 1991.
15. T. Tozaki, K. Yoshiki, N. Noboru, O. Hironobu, R. Kakinuma, K. Eguchi, M. Kaneko, and N. Moriyama, "Pulmonary Organs Analysis Method and Its Application to Differential Diagnosis Based on Thoracic Thin-Section CT Images," in *Medical Imaging (Proceedings of SPIE)*, 3338, pp. 1459-1669, San Diego, California, 1998.
16. J. H. Woodring, and A. M. Frued, "Significance of Wall Thickness in Solitary Cavities of the Lung: A Follow-Up Study", *American Journal of Roentgenology*, 140(3), pp. 473-474, 1983.

Feature Extraction, Analysis, and 3D Visualization of Local Lung Regions in Volumetric CT Images

Andrzej Delegacz[a,b], Shih-Chung B. Lo[a], Matthew T. Freedman[a], and Seong K. Mun[a]

[a]ISIS Center, Georgetown University Medical Center, Washington, DC
[b]Department of Electrical Engineering, Catholic University of America, Washington, DC

ABSTRACT

The purpose of the work was to develop image functions for volumetric segmentation, feature extraction, and enhanced 3-dimensional visualization of local regions using CT datasets of human lungs. The system is aimed to assist the radiologist in the analysis of lung nodules. Volumetric datasets consisting of 30-50 thoracic helical low-dose CT slices were used in the study. The 3D topological characteristics of local structures including bronchi, blood vessels, and nodules were computed and evaluated. When a location of a region of interest is identified, the computer would automatically compute size, surface of the area, and normalized shape index of the suspected lesion. The developed system can also allow the user to perform interactive operation for evaluation of lung regions and structures through a user-friendly interface. These functions provide the user with a powerful tool to observe and investigate clinically interesting regions through unconventional radiographic viewings and analyses. The developed functions can also be used to view and analyze patient's lung abnormalities in surgical planning applications. Additionally, we see the possibility of using the system as a teaching tool for correlating anatomy of lungs.

Keywords: real-time 3D visualization, 3D feature extraction, medical imaging, helical CT, image filtering, image segmentation, normalized shape index, image processing, volume rendering, lung nodule detection.

1. INTRODUCTION

For a considerable number of years, lung cancer has been ranked as the leading cause of cancer death worldwide. This statistical result is also applicable to American men and women. In the US alone, it is estimated that lung cancer causes a total of 157,000 deaths annually, with a 5-year survival rate of 13% when all stages are considered[1]. Screening with CT has been shown to enable the detection of lung cancers smaller than those detected on chest radiographs[2,3]. The application of CT imaging may be beneficially used in the diagnosis of smokers and former smokers, who constitute a large population at risk for lung cancer. As many as 60 million current and former smokers at risk are thought to comprise this population.

Early detection of lung cancer in a screening program may be possible but new tools and technical skills are needed for the effort to be effective. A great number of pulmonary radiologists using state-of-the-art radiographic tools will be required to participate. In addition, such a screening program will require a well-planned clinical protocol as well as a health care policy supported by the society in which the smokers and former smokers reside. Given the very large potential volume of such studies, methods of assisted interpretation should be in great demand.

The trend of using helical CT as a clinical tool for screening lung cancer addresses four focuses:(1) an alternative to the low sensitivity of chest radiography, (2) the development of higher throughput low-dose helical CT, (3) the potential cost reduction of helical CT systems, and (4) the development of a computer diagnostic system as an aid for pulmonary radiologists. One can anticipate that the cost of each CT examination will still be higher than that of conventional chest x-rays. However, for a high-risk population, the greater capability of this imaging modality to detect early lung cancer may outweigh its costs.

Given the frequencies of false positive detections in both Japan and the US, the frequency of false negative exams in Japan, and the frequency of thoracotomy finding only benign disease, we consider that there is a pressing need for improved diagnostic methods to be developed now, as the use of screening CT is rapidly increasing and will result in many unnecessary procedures. Computer algorithms have been shown to increase sensitivity and/or specificity in the detection of lung cancer on chest radiographs and breast cancer on mammography. Application of these methods to screening CT is appropriate.

Since lung cancer continues to exact a significant toll on the American population, and other methods of early detection have had only limited success, we consider continued efforts to improve the accuracy of interpretation of helical CT images and chest radiographs to be quite important. The helical CT represents an advanced clinical tool for high-risk patients. The chest radiograph continues to be the clinical tool for lung cancer detection whether in symptomatic or asymptomatic patients.

In recent years, increasing number of 3-D visualization systems have become available as both research tools and commercial products. Most of those systems provide the users with display functions such as lightbox (2D) and volume rendering (3D) views, color and opacity transfer functions, lighting and shading, volume cropping, etc. These functions are somewhat too general to be used in lung cancer diagnosis. We therefore begin to conduct research and development of clinically useful functions as tools tailored for thoracic CT images. In the past, we have presented image functions including automatic lung segmentation, slice interpolation, and 3D display of the segmented lungs of CT scans[4]. In this paper, we further present segmentation of nodules, isolation of bronchial patterns, and 3D display as well as feature analysis for the local regions.

2. VISUALIZATION

The main concept behind the design of our system is to allow for interactive selection of the region of interest (ROI) and further investigation of its contents in details as well as obtaining the quantitative feature characteristics of selected structures. Since the ultimate structures to be visualized and measured are rather small comparing to the overall lung volume, the system is designed to make the selection as easy and flexible as possible whereas maintaining user's complete control over the system. To this end we implement two-stage ROI selection procedure. A user is presented with the volume-rendered view of the whole lung volume in a small window ("preview window"). Selection of the ROI that will be further investigated, is made by using a 3D cursor and pointing at the location of interest. This mode of operation is called the preview mode. A portion of visualization pipeline that implements the preview mode is presented in Figure 1. A content of the preview window is shown in Figure 2.

The location of the 3D cursor in the preview window is synchronized with the contents of two other large windows in which the magnified volume-rendered ("detail volume rendering window") and surface-rendered ("detail surface rendering window") views of the selected ROI are displayed. In this mode, called the detail mode, the user utilizes another 3D cursor to move the small probe volume that selects the "structure of interest" (SOI) that undergoes further feature extraction and analysis. Although not directly involved in processing related to feature extraction, the volume-rendered view in detail mode can be a useful tool that provides an insight for the user to look into tissues and structures comprising the ROI and supporting effective search of regions worth further exploration. A volumetric rendering pipeline for presenting detail lung structures has been implemented as depicted in Figure 3. Examples of images displayed in this view are presented in Figure 4.

The surface-rendered view of the detailed mode uses the techniques of isosurface contouring combined with 3D mesh extraction to generate the 3D surface out of the volumetric data available from the volume rendering portion of the visualization pipeline. The resulting image is displayed in the detail surface rendering window. The user-operated small cube or sphere probe volume picks up the part of the 3D surface that represents the SOI. This data is passed to the feature extraction and analysis module of the system and is used to perform defined feature calculations. Both the isosurface contouring threshold and the probe parameters may be easily changed by the user in an interactive manner. The diagram of the surface rendering part of the detail mode visualization pipeline is shown in Figure 5. Figure 6 presents an example content of detail surface rendering window corresponding to the ROI and SOI shown in previous pictures (Figures 2 and 4).

3. FEATURE EXTRACTION

The data flow in the system is designed to pass the 3D surface mesh data of the SOI from the visualization pipeline to the feature extraction module. The 3D surface mesh data can be used for extraction and calculation of a number of features of small structures under evaluation. In this work, we intended to develop a full processing and visualization paths for getting the feature extraction results from the CT scan volume dataset rather than developing the complete feature extraction and analysis system. Specifically, the features of the SOI within the probe in the detailed mode are automatically computed. With today PC speed, real-time feature values can be obtained even with on-line manipulation of the probe location, probe size/shape, and isosurface contouring threshold value:
- Surface area – total area of the surface of the structure of interest;
- Volume – volume of the structure of interest;
- Normalized shape index – non-dimensional parameter calculated by dividing the cube root of the volume by the square root of the area divided by 2.199. This normalizes the value to 1.0 for a sphere.
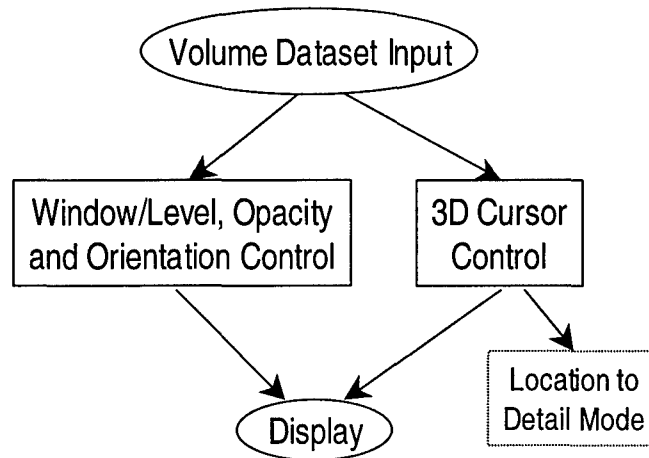
Figure 1. A diagram of the preview mode portion of the system visualization pipeline.
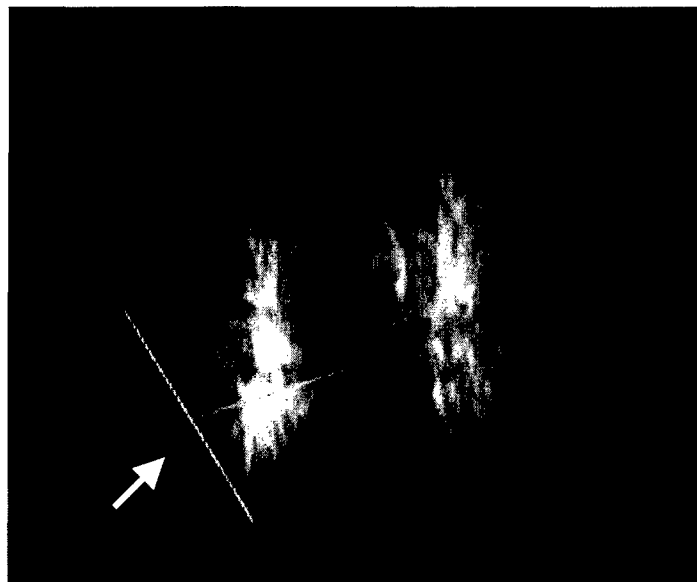

Figure 2. An image of the whole lung volume rendered in the preview window. The lines of 3D cursor (displayed in red, green and blue on the color monitor) are visible in the lower left-hand corner of the picture (indicated with the white arrow).
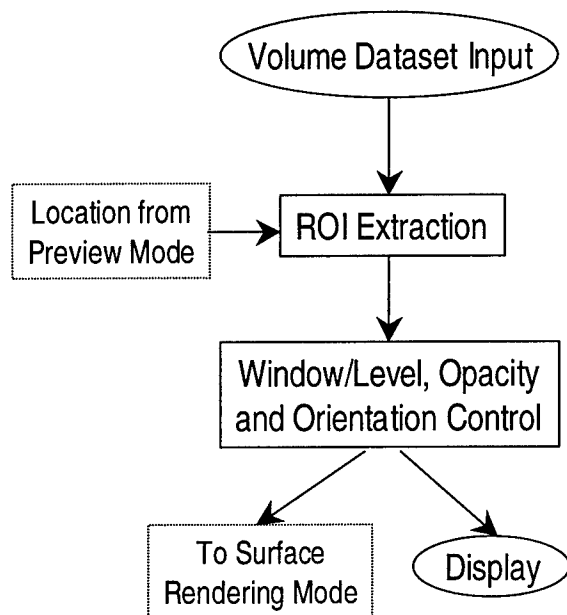
Figure 3. A diagram of the volume rendering part of detail mode portion of the system visualization pipeline.
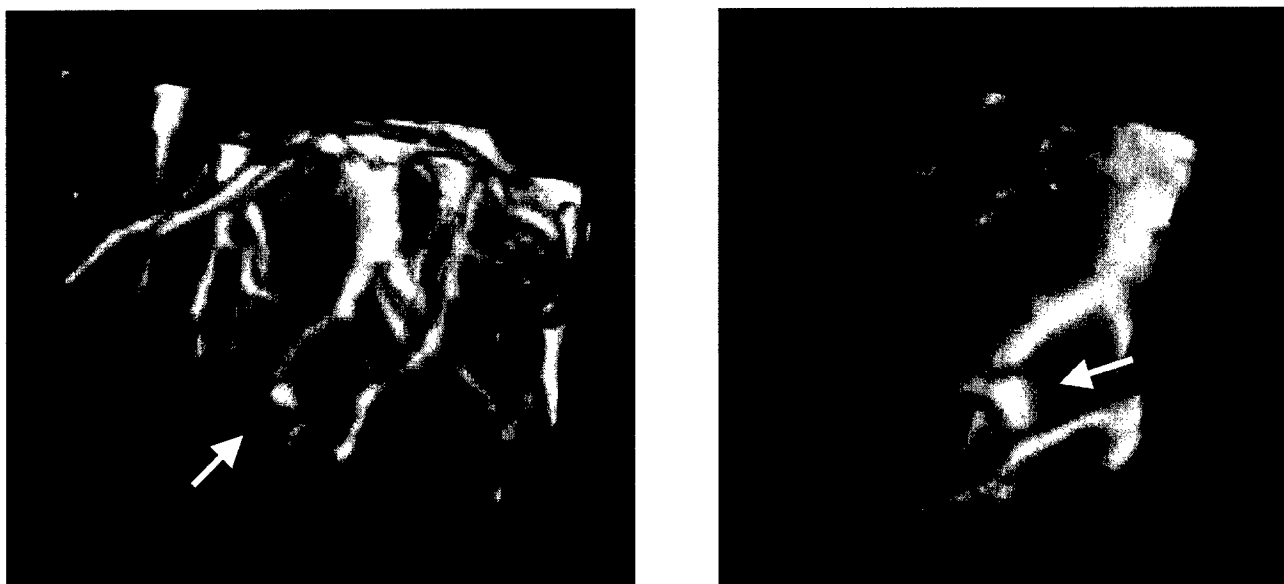

Figure 4. Two images of the same region of interest (selected with the 3D cursor in the preview mode – see Figure 2) displayed in the detail volume rendering window. The image on the right side has been additionally magnified and rotated to better show the suspected nodule. The white arrows on both images indicate the structure of interest that will be further processed in the surface-rendered detail mode.
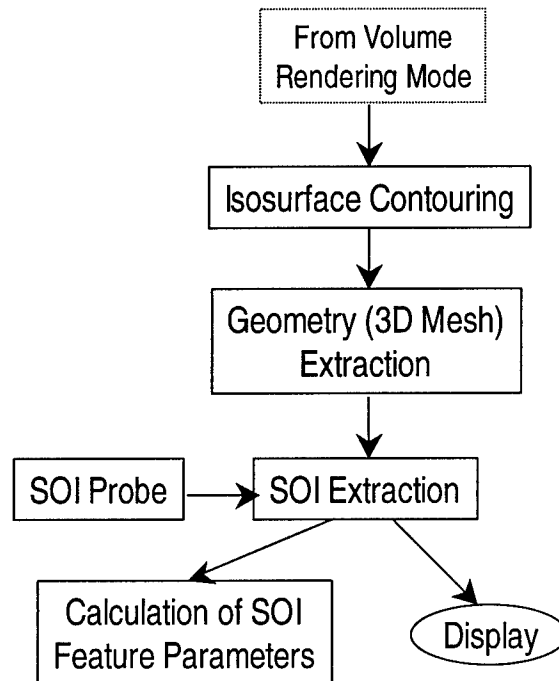
Figure 5. A diagram of the surface rendering part of detail mode portion of the system visualization pipeline.
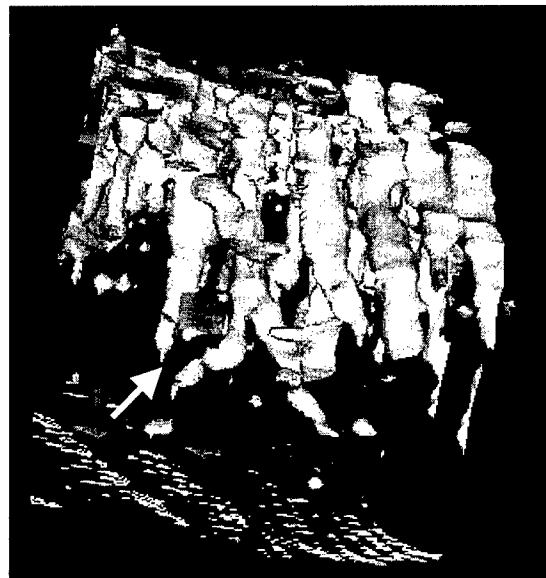

Figure 6. The image of the region of interest (same as the one shown in Figure 4) displayed in the detail surface rendering window. The white arrow indicates the cube probe volume (displayed in red on the color monitor) selecting the structure of interest which features are calculated in the feature extraction and analysis module.

4. CONCLUSIONS AND DISCUSSION

Diagnostic viewing requires a high-resolution CT scan with or without a contrast agent5. With regard to the diagnosis of solitary pulmonary nodules6, specific features to assess the nodules on CT images include: (1) size and location, (2) margins and boundaries, (3) vessels and bronchi, (4) cavitation, (5) satellite nodules, and (6) density. 3D view with advanced image processing techniques (e.g. enhanced bronchi, arteries, and veins) will assist the radiologist in analysis of the characteristics of tumor margins, its association with vessels and bronchi, the wall thickness of tumor cavitation, and density level and uniformity of the tumor.

We believe, therefore, that the proposed viewing methods will be of great value for (1) rapid viewing in screening and diagnostic CT while cooperating with a computer-aided detection system and (2) enhancing clinical capability in assessing the property of the tumor while cooperating with a computer-aided diagnosis system. The goals of this work are to (a) explore clinically useful display methods for viewing and diagnosis of lung images of CT, (b) establish an advanced display workstation for clinical evaluation, and (c) form a technical base to facilitate the development of computer-aided systems.

With the availability of a computer-aided detection algorithm in the viewing system, suspected areas can be highlighted in 3D display to provide the radiologist with rapid and clear 3D geometrical information for the evaluation of suspected lung nodules. Based on the computer-aided system development in this area so far, visual evaluation is necessary to determine clinically significant detections among those detected and undetected by the computer.

The designed and implemented prototype of the 3D visualization system gives the user a unique new way to conduct fast and effective observation of small lung structures including potential lung abnormalities and cancer nodules. The feature extraction module fully integrated with of the system serves as a powerful tool for in-depth quantitative analysis of those small structures and fully integrates with the visualization part of the system according to the paradigm "what you see is what you measure". We expect that the developed system can be used to view and analyze volume datasets of thoracic CT images in a new powerful way in both screening and diagnostic applications. Additionally, we see the possibility of using the system for teaching anatomy of the human lungs.

The main part of the system visualization pipeline was developed using Kitware VTK software package (version 3.2 beta)7. The user interface was created in Java (Sun Microsystems Java2 SDK 1.3). The integrated pre-processing (interpolation, segmentation) as well as feature extraction and analysis modules were developed using authors' original algorithms implemented in C and C++. The system is designed for a PC platform powered by Intel Pentium III processor running Microsoft Windows 95/98/NT/2000 operating systems.

5. ACKNOWLEDGEMENTS

6. REFERENCES

1. P. A. Wingo, T. Tong , and S. Bolden, "Cancer statistics 1995," CA: A Cancer Journal for Clinicians., 45, pp. 8-30, 1995.
2. C. I. Henschke, D. I. McCauley, D. F. Yankelevitz, et al., "Early Lung Cancer Action Project: Overall Design and Findings from Baseline Screening," The Lancet, 354, pp. 99-105, 1999.
3. T. Iinuma, Y. Tateno, T. Matsumoto, S. Yamamoto, and M. Matsumoto, "Basic Idea of Lung Cancer Screening CT (LSCT) and its Preliminary Evaluation," Jap. J Radio Med, 52(2), pp. 182-190, 1992.
4. A. Delegacz, S. C. Lo, H. Xie, M. T. Freedman, and J. J. Choi, "Three-Dimensional Visualization System as an Aid for Lung Cancer Diagnosis," in Medical Imaging (Proceedings of SPIE), 3976, pp. 401-409, San Diego, California, 2000.
5. T. Tozaki, K. Yoshiki, N. Noboru, O. Hironobu, R. Kakinuma, K. Eguchi, M. Kaneko, and N. Moriyama, "Pulmonary Organs Analysis Method and Its Application to Differential Diagnosis Based on Thoracic Thin-Section CT Images," in Medical Imaging (Proceedings of SPIE), 3338, pp. 1459-1669, San Diego, California, 1998.
6. J. H. Woodring, and A. M. Frued, "Significance of Wall Thickness in Solitary Cavities of the Lung: A Follow-Up Study," American Journal of Roentgenology, 140(3), pp. 473-474, 1983.
7. W. J. Schroeder, K. M. Martin, L. S. Avila, and C. C. Law, "The Visualization Toolkit User's Guide," Kitware, Inc., 2000

MCMR-RMI-S   (70-1y)   11 Mar 03

MEMORANDUM FOR Administrator, Defense Technical Information
Center (DTIC-OCA), 8725 John J. Kingman Road, Fort Belvoir,
VA 22060-6218

SUBJECT: Request Change in Distribution Statement

1. The U.S. Army Medical Research and Materiel Command has
reexamined the need for the limitation assigned to technical
reports written for this Command. Request the limited
distribution statement for the enclosed accession numbers be
changed to "Approved for public release; distribution unlimited."
These reports should be released to the National Technical
Information Service.

2. Point of contact for this request is Ms. Kristin Morrow at
DSN 343-7327 or by e-mail at Kristin.Morrow@det.amedd.army.mil.

FOR THE COMMANDER:

Encl   PHYLIS M. RINEHART
                                        Deputy Chief of Staff for
                                        Information Management

ADB264655
ADB282172
ADB261548
ADB282212
ADB282747
ADB282213
ADB282133
ADB282748
ADB282793
ADB282229
ADB282720
ADB282132